

Bayesian Density-Density Regression with Application to Cell-Cell Communications

Khai Nguyen¹, Yang Ni^{1,2}, and Peter Mueller^{1,3}

¹Department of Statistics and Data Sciences, University of Texas at Austin

²Department of Statistics, Texas A&M University

³Department of Mathematics, University of Texas at Austin

April 18, 2025

Abstract

We introduce a scalable framework for regressing multivariate distributions onto multivariate distributions, motivated by the application of inferring cell-cell communication from population-scale single-cell data. The observed data consist of pairs of multivariate distributions for ligands from one cell type and corresponding receptors from another. For each ordered pair $e = (l, r)$ of cell types ($l \neq r$) and each sample $i = 1, \dots, n$, we observe a pair of distributions (F_{ei}, G_{ei}) of gene expressions for ligands and receptors of cell types l and r , respectively. The aim is to set up a regression of receptor distributions G_{ei} given ligand distributions F_{ei} . A key challenge is that these distributions reside in distinct spaces of differing dimensions. We formulate the regression of multivariate densities on multivariate densities using a generalized Bayes framework with the sliced Wasserstein distance between fitted and observed distributions. Finally, we use inference under such regressions to define a directed graph for cell-cell communications.

Keywords: Multivariate Density-Density Regression, Generalized Bayes, Optimal Transport, Sliced Wasserstein.

1 Introduction

We propose the first approach for regressing random distributions on random distributions in *multivariate settings*. A key feature of our approach, which is Bayesian, is its ability to provide a full probabilistic characterization of all relevant unknowns, including data and model parameters. However, this feature can also become a limitation, particularly when dealing with complex relationships in which specifying a complete probabilistic model is challenging. To address this, we adopt a generalized Bayes framework that circumvents the need to fully specify likelihoods. Our approach leverages the sliced Wasserstein distance to measure the discrepancy between the observed response distribution and the predicted distribution, allowing for a principled update of beliefs while maintaining flexibility.

In the usual regression setup, both the predictors and responses are typically scalars or vectors. When distributional variables serve as the predictors and real-valued variables as the response, the density regression problem arises (Póczos et al., 2013), e.g., predicting health indicators from a distribution of clinical outcomes (Szabó et al., 2016) or estimating the effects of physical activity on biomarkers (Matabuena and Petersen, 2023). Another type of density regression arises with real-valued predictors and density-valued responses. This is studied, for example, in Tokdar et al. (2004); Dunson et al. (2007) or Shen and Ghosal (2016). Recently, the density-density regression (DDR) problem, which deals with distributional predictor and distributional response variables, has been studied. For example, regression with one-dimensional predictor and one-dimensional response is considered in Zhao et al. (2023) using a Riemannian representation of density functions. The method of Zhao et al. (2023) is hard to extend to *multivariate* settings due to the usage of a wrapping function, which is only well-defined in one dimension. To the best of our knowledge, there are currently no methods for DDR with *multivariate* distributions.

We propose a DDR model, where both predictors and responses are random distributions of arbitrary dimensions. The motivation comes from the challenge of modeling molecular dependence relationships among different cell types in population-scale single-cell data. In this type of data, gene expressions are measured for a large number of cells donated by a large number of subjects. Exploiting that cell types can be identified based on known cellular markers, this provides an opportunity to decipher the communication patterns between different cell types by way of expressions of ligand-receptor pairs. Because of the availability of a large number of cells from each donor, we, in essence, observe for each subject the empirical distributions of the gene expressions for each cell type. Therefore, we can cast the inference problem of cell-cell communications as a DDR problem, where the predictor for each subject is the distribution of gene expression for the ligands from one cell type and the response is the distribution for receptors from another cell type. Conventional bulk gene expression methods collapse the distributional representation by taking the mean as the representative statistic for downstream regression. In contrast, the proposed Bayesian DDR approach allows us to model complex regression dependencies between distributions while preserving the full variability and uncertainty of the data.

Our inference procedure is based on the posterior distribution for a regression function that maps from the space of the predictor distribution to the space of the response distribution. Avoiding an explicit sampling model, we rely instead on a *generalized likelihood*, which is constructed based on a discrepancy between the pushforward (predicted) response distribution and the observed response distribution. Hence, the proposed Bayesian DDR approach falls within the generalized Bayesian inference framework (Bissiri et al., 2016).

One challenge in implementing DDR is that we do not directly observe distributions through their density functions. Instead, we observe *finite* samples from distributions.

Moreover, the number of observed samples can differ between distributions, and distributions may lie in high-dimensional spaces. Therefore, for the construction of the generalized likelihood we need to use a discrepancy between distributions that can be reliably estimated with *finite* samples in high dimensions. We choose the sliced Wasserstein distance (Rabin et al., 2012; Bonneel et al., 2015; Peyré et al., 2019), which is a sliced variant (random projection variant) of the Wasserstein distance (Villani, 2009). Sliced Wasserstein does not suffer from the curse of dimensionality and is computationally scalable with respect to the number of support points in the distributions. Moreover, the use of sliced Wasserstein allows us to derive a Metropolis-adjusted Langevin algorithm (MALA, Girolami and Calderhead 2011) for efficient inference.

Using the proposed Bayesian DDR, we construct a cell-cell communication network of different cell types based on ligand–receptor interactions for each pair of cell types. We perform Bayesian DDR for each pair of cell types, i.e., regressing distributions over receptors onto distributions over ligands. After fitting the Bayesian DDR models, we propose two ways to infer a network. The first option is a weighted fully-connected graph with edge weights derived from the expected relative errors of the regressions. The second approach casts the graph selection as a decision problem, which we implement by way of a simple decision boundary. In particular, we parameterize the regression as a linear function and put a shrinkage prior on the linear coefficient. We report edges by thresholding the posterior probabilities in these linear functions, with the threshold determined by minimizing posterior expected false negative rate (FNR) under a bound on posterior expected false discovery rate (FDR).

The remainder of the article is organized as follows. In Section 2, we review the definitions of Wasserstein and sliced Wasserstein distance, and their statistical and computational

properties. In Section 3, we propose a generalized Bayesian DDR framework using sliced Wasserstein distance to define a generalized likelihood, and we derive posterior simulation using a MALA sampler. In Section 4, we apply the proposed Bayesian DDR approach to infer cell-cell communication between two cell types. In Section 5, we build on the regression setup and propose discovery of a directed graph by way of forming Bayesian DDRs for ordered pairs of cell types. In Section 6, we apply the proposed graph discovery for graphs among multiple cell types in a population-scale single-cell dataset, and we validate inference in a semi-simulation with real predictor distributions and a simulated true regression function.

For notations, we use δ_x to denote the Dirac delta function, which takes the value 1 at x and 0 otherwise. For any $d \geq 2$, we denote $\mathbb{S}^{d-1} = \{\theta \in \mathbb{R}^d \mid \|\theta\|_2^2 = 1\}$ as the unit hypersphere. We use I for the identity matrix and $\mathbf{1}$ for the vector of all 1's, with the size depending on the context. For any two sequences a_n and b_n , the notation $a_n = \mathcal{O}(b_n)$ means that $a_n \leq Cb_n$ for all $n \geq 1$, where C is some universal constant. Other notations will be introduced later when they are used.

2 Background on Sliced Wasserstein Distance

By way of a brief review of sliced Wasserstein distance, we introduce some notation and definitions. Given $p \geq 1$, let $G_1, G_2 \in \mathcal{P}_p(\mathbb{R}^d)$ where $\mathcal{P}_p(\mathbb{R}^d)$ be the set of all distributions supported on the \mathbb{R}^d with finite p -th moment. Wasserstein- p ($p \geq 1$) distance (Villani, 2009) between G_1 and G_2 is defined as:

$$W_p^p(G_1, G_2) = \inf_{\pi \in \Pi(G_1, G_2)} \int_{\mathbb{R}^d \times \mathbb{R}^d} \|x - y\|_p^p d\pi(x, y), \quad (1)$$

where $\Pi(G_1, G_2) = \{\pi \in \mathcal{P}(\mathbb{R}^d \times \mathbb{R}^d) \mid \pi(A, \mathbb{R}^d) = G_1(A), \pi(\mathbb{R}^d, B) = G_2(B) \forall A, B \subset \mathbb{R}^d\}$ is the set of all transportation plans/couplings. When observing $x_1, \dots, x_{m_1} \stackrel{i.i.d.}{\sim} G_1$ and $y_1, \dots, y_{m_2} \stackrel{i.i.d.}{\sim} G_2$, the plug-in estimation of the Wasserstein- p distance is given by:

$$W_p^p(G_{1,m_1}, G_{2,m_2}) = \min_{\gamma \in \Gamma(\mathbf{1}/m_1, \mathbf{1}/m_2)} \sum_{i=1}^{m_1} \sum_{j=1}^{m_2} \|x_i - y_j\|_p^p \gamma_{ij}, \quad (2)$$

where $G_{1,m_1} = \frac{1}{m_1} \sum_{i=1}^{m_1} \delta_{x_i}$ and $G_{2,m_2} = \frac{1}{m_2} \sum_{j=1}^{m_2} \delta_{y_j}$ are corresponding empirical distributions over i.i.d. samples from G_1 and G_2 , and the set of discrete transportation plans is $\Gamma(\mathbf{1}/m_1, \mathbf{1}/m_2) = \{\gamma \in \mathbb{R}_+^{m_1 \times m_2} \mid \gamma \mathbf{1} = \mathbf{1}/m_1, \gamma^\top \mathbf{1} = \mathbf{1}/m_2\}$. Computing $W_p^p(G_{1,m_1}, G_{2,m_2})$ is a linear programming problem, which costs $\mathcal{O}((m_1 + m_2)^3 \log(m_1 + m_2))$ in time complexity (Peyré et al., 2019). From Fournier and Guillin (2015), we have the following sample complexity: $\mathbb{E}[|W_p(G_{1,m_1}, G_{2,m_2}) - W_p(G_1, G_2)|] = \mathcal{O}(m_1^{-1/d} + m_2^{-1/d})$, which implies that we need m_1 and m_2 to be large to achieve small approximation errors. However, the time complexity to compute the Wasserstein distance scales poorly with m_1 and m_2 .

This conundrum is addressed by introducing sliced Wasserstein (SW) distance (Rabin et al., 2014; Bonneel et al., 2015). SW relies on the fact that one-dimensional Wasserstein distance can be computed efficiently. In particular, let $G_1, G_2 \in \mathcal{P}_p(\mathbb{R})$, computing $W_p^p(G_{1,m_1}, G_{2,m_2})$ in Equation (2) costs only $\mathcal{O}((m_1 + m_2) \log(m_1 + m_2))$ in time complexity by using the north-west corner solution (Peyré et al., 2019).

SW distance between two distributions $G_1, G_2 \in \mathcal{P}_p(\mathbb{R}^d)$ is defined as: $SW_p^p(G_1, G_2) = \mathbb{E}_{\theta \sim \mathcal{U}(\mathbb{S}^{d-1})}[W_p^p(\theta \# G_1, \theta \# G_2)]$, where $\mathcal{U}(\mathbb{S}^{d-1})$ is the uniform distribution over the unit hypersphere in d dimension, and $\theta \# G_1$ and $\theta \# G_2$ denote the pushforward distribution of G_1 and G_2 through the function $f_\theta(x) = \theta^\top x$. In particular, given two measurable spaces $(\mathcal{X}_1, \Sigma_1)$ and $(\mathcal{X}_2, \Sigma_2)$, a measurable function $f : \mathcal{X}_1 \rightarrow \mathcal{X}_2$, and a measure $\mu : \Sigma_1 \rightarrow [0, \infty)$, the pushforward of μ through f is $f \# \mu(B) = \mu(f^{-1}(B))$ for any $B \in \Sigma_2$ – we will use the

definition with probability measures only. Similar to Wasserstein, we have the following plug-in estimation of SW:

$$SW_p^p(G_{1,m_1}, G_{2,m_2}) = \mathbb{E}_{\theta \sim \mathcal{U}(\mathbb{S}^{d-1})} [W_p^p(\theta^\# G_{1,m_1}, \theta^\# G_{2,m_2})]. \quad (3)$$

From Nadjahi et al. (2020); Nguyen et al. (2021); Nietert et al. (2022); Boedihardjo (2025), we have that $\mathbb{E}[|SW_p(G_{1,m_1}, G_{2,m_2}) - SW_p(G_1, G_2)|] = \mathcal{O}(m_1^{-1/2} + m_2^{-1/2})$. In particular, there is no dimension dependence. Combining with the linear-time complexity of empirical SW, we have a both, computationally and statistically, scalable solution for comparing distributions. The last step to compute SW is approximating the expectation with respect to $\mathcal{U}(\mathbb{S}^{d-1})$ (Nguyen et al., 2024; Leluc et al., 2024; Nguyen and Ho, 2024; Sisouk et al., 2025). For example, we can use a simple Monte Carlo estimation:

$$\widehat{SW}_p^p(G_{1,m_1}, G_{2,m_2}; L) = \frac{1}{L} \sum_{l=1}^L W_p^p(\theta_l^\# G_{1,m_1}, \theta_l^\# G_{2,m_2}), \quad (4)$$

where $\theta_1, \dots, \theta_L \stackrel{i.i.d.}{\sim} \mathcal{U}(\mathbb{S}^{d-1})$ with L being the number of Monte Carlo samples or the number of projections. The overall time complexity for computing this approximation is $\mathcal{O}(L(m_1+m_2) \log(m_1+m_2) + Ld(m_1+m_2))$ where $\mathcal{O}(Ld(m_1+m_2))$ is for projecting supports of G_{1,m_1} and G_{2,m_2} , and $\mathcal{O}(L(m_1+m_2) \log(m_1+m_2))$ is for computing $W_p^p(\theta_l^\# G_{1,m_1}, \theta_l^\# G_{2,m_2})$ with $\theta_l^\# G_{1,m_1} = \frac{1}{m_1} \sum_{i=1}^{m_1} \delta_{\theta_l^\top x_i}$ and $\theta_l^\# G_{2,m_2} = \frac{1}{m_2} \sum_{j=1}^{m_2} \delta_{\theta_l^\top y_j}$ for $l = 1, \dots, L$.

3 Generalized Bayesian Density-Density Regression

3.1 Generalized Bayesian Density-Density Regression

We consider the inference problem of relating a distribution-valued response G_i to a distribution-valued predictor F_i . We observe samples $x_{i1}, \dots, x_{im_{i1}} \sim F_i \in \mathcal{P}_2(\mathbb{R}^{d_1})$ and $y_{i1}, \dots, y_{im_{i2}} \sim G_i \in \mathcal{P}_2(\mathbb{R}^{d_2})$ for $i = 1, \dots, N$. Let $\mathcal{S} = \{(\{x_{i1}, \dots, x_{im_{i1}}\}, \{y_{i1}, \dots, y_{im_{i2}}\})\}_{i=1}^N$ denote the observed data where $x_{i1}, \dots, x_{im_{i1}} \in \mathbb{R}^{d_1}$ and $y_{i1}, \dots, y_{im_{i2}} \in \mathbb{R}^{d_2}$. Equivalently, we represent the data as $\mathcal{S} = \{(\hat{F}_i, \hat{G}_i)\}_{i=1}^N$ where $\hat{F}_i = \frac{1}{m_{i1}} \sum_{j=1}^{m_{i1}} \delta_{x_{ij}}$ and $\hat{G}_i = \frac{1}{m_{i2}} \sum_{j=1}^{m_{i2}} \delta_{y_{ij}}$ are the empirical distributions. Assuming large enough sample sizes m_{i1} and m_{i2} , we drop the distinction of (F_i, G_i) versus (\hat{F}_i, \hat{G}_i) .

We define the following DDR model:

$$G_i | F_i, f \sim p(G_i | F_i, f) \propto \exp \left(-w \sum_{i=1}^N \widehat{SW}_2^2(f \# F_i, G_i; L) \right), \quad (5)$$

where f is a measurable function that maps from \mathbb{R}^{d_1} to \mathbb{R}^{d_2} , $L \geq 1$, and $w > 0$. The likelihood $p(G_i | F_i, f)$ in (5) is a *generalized likelihood* (Bissiri et al., 2016).

In (5) we are using SW distance to define a loss function that serves as generalized (negative log) likelihood. SW is an attractive choice for the loss function as it naturally defines a distance between random distributions $f \# F_i$ and G_i . One of the advantages of using the generalized likelihood is that it sidesteps the need for a full probabilistic description of all relevant unknowns. If desired, the SW distance between two empirical distributions can be replaced by the SW distance between any alternative estimates of F_i and G_i , for example, using kernel density estimates or a fitted mixture of Gaussians. For simplicity, we choose to use empirical distributions. Also, SW distance, which relies on Euclidean geometry, can be replaced with other variants of SW (Kolouri et al., 2019) if

more information about the geometry of the distributions were available.

To assess goodness of fit, we use the following predictive error between the fitted distribution and the recorded response distributions: $PE(\mathcal{S}, L) = \frac{1}{N} \sum_{i=1}^N \widehat{SW}_2^2(f \# F_i, G_i; L)$, which can be calculated by posterior samples. Given $f_1, \dots, f_T \sim p(f \mid \mathcal{S})$, we have the following approximated mean predictive error: $\overline{PE}(\mathcal{S}, L) = \frac{1}{T} \frac{1}{N} \sum_{t=1}^T \sum_{i=1}^N \widehat{SW}_2^2(f_t \# F_i, G_i; L)$. Assume we have a reference model f_0 that serves as a worst-case reference (see later for examples), which is similar to an intercept-only model in a linear regression. We normalize the relative error to obtain the following relative predictive error (RPE):

$$\text{RPE}(\mathcal{S}, L) = \frac{1}{N} \sum_{i=1}^N \frac{\widehat{SW}_2^2(f \# F_i, G_i; L)}{\widehat{SW}_2^2(f_0 \# F_i, G_i; L)}. \quad (6)$$

Similarly, the mean RPE can be estimated using posterior samples, i.e.,

$$\overline{\text{RPE}}(\mathcal{S}, L) = \frac{1}{T} \frac{1}{N} \sum_{t=1}^T \sum_{i=1}^N \frac{\widehat{SW}_2^2(f_t \# F_i, G_i; L)}{\widehat{SW}_2^2(f_{0t} \# F_i, G_i; L)}, \quad (7)$$

where posterior samples $f_1, \dots, f_T \sim p(f \mid \mathcal{S})$ and posterior samples $f_{01}, \dots, f_{0T} \sim p(f_0 \mid \mathcal{S})$. Later, in the case where f takes a linear form, we will define f_0 as an intercept model.

3.2 Posterior Inference

Posterior inference under (5) is based on the generalized posterior,

$$p(f \mid \mathcal{S}) \propto p(f) \exp \left(-w \sum_{i=1}^N \widehat{SW}_2^2(f \# F_i, G_i; L) \right), \quad (8)$$

where $p(f)$ is a prior distribution of f . We implement inference by Markov chain Monte Carlo (MCMC) simulation from (8). For computational efficiency, we restrict the function

f to a parametric form, i.e., f_ϕ with parameters $\phi \in \Phi$. Given a prior $p(\phi)$, we have the generalized posterior:

$$p(\phi \mid \mathcal{S}) \propto p(\phi) \exp \left(-w \sum_{i=1}^N \widehat{SW}_2^2(f_\phi \# F_i, G_i; L) \right). \quad (9)$$

We restrict the function f_ϕ and $\log\{p(\phi)\}$ to be differentiable with respect to ϕ to facilitate the use of gradient-based MALA (one-step hybrid Monte Carlo) transition probabilities using the following proposal distribution: $q(\phi' \mid \phi) \propto \exp \left(-\frac{1}{4\eta} \|\phi' - \phi - \eta \nabla_\phi \log p(\phi \mid \mathcal{S})\|_2^2 \right)$, for a fixed step size $\eta > 0$. We sample $\phi' \sim q(\phi' \mid \phi)$ as $\phi' = \phi + \eta \nabla_\phi \log p(\phi \mid \mathcal{S}) + \sqrt{2\eta} \epsilon_0$, with $\epsilon_0 \sim \mathcal{N}(0, I)$, a standard multivariate Gaussian distribution of dimension matching the parameter ϕ . We accept ϕ' with probability: $\alpha = 1 \wedge p(\phi \mid \mathcal{S})q(\phi \mid \phi') / (p(\phi' \mid \mathcal{S})q(\phi' \mid \phi))$.

We now derive the gradient $\nabla_\phi \log p(\phi \mid \mathcal{S}) = \nabla_\phi \log p(\phi) - w \sum_{i=1}^N \nabla_\phi SW_p^2(f_\phi \# F_i, G_i)$, where $\nabla_\phi \widehat{SW}_2^2(f_\phi \# F_i, G_i; L) = \frac{1}{L} \sum_{l=1}^L \nabla_\phi W_2^2(\theta_l \# f_\phi \# F_i, \theta_l \# G_i)$ with

$$\nabla_\phi W_2^2(\theta_l \# f_\phi \# F_i, \theta_l \# G_i) = \nabla_\phi \left(\min_{\gamma \in \Gamma(\mathbf{1}/m_{i1}, \mathbf{1}/m_{i2})} \sum_{i'=1}^{m_{i1}} \sum_{j'=1}^{m_{i2}} (\theta_l^\top f_\phi(x_{ii'}) - \theta_l^\top y_{ij'})^2 \gamma_{i'j'} \right). \quad (10)$$

Since the function $\sum_{i'=1}^{m_{i1}} \sum_{j'=1}^{m_{i2}} (\theta^\top f_\phi(x_{ii'}) - \theta^\top y_{ij'})^2$ is continuous in ϕ and the set of discrete transportation plans $\Gamma(\mathbf{1}/m_{i1}, \mathbf{1}/m_{i2})$ is a compact set, we can apply Danskin's envelope theorem with $\gamma^* = \operatorname{argmin}_{\gamma \in \Gamma(\mathbf{1}/m_{i1}, \mathbf{1}/m_{i2})} \sum_{i'=1}^{m_{i1}} \sum_{j'=1}^{m_{i2}} (\theta^\top f_\phi(x_{ii'}) - \theta^\top y_{ij'})^2 \gamma_{i'j'}$ and obtain the gradient:

$$\begin{aligned} \nabla_\phi \left(\min_{\gamma \in \Gamma(\frac{1}{m_{i1}}, \frac{1}{m_{i2}})} \sum_{i'=1}^{m_{i1}} \sum_{j'=1}^{m_{i2}} (\theta^\top f_\phi(x_{ii'}) - \theta^\top y_{ij'})^2 \gamma_{i'j'} \right) &= \nabla_\phi \left(\sum_{i'=1}^{m_{i1}} \sum_{j'=1}^{m_{i2}} (\theta^\top f_\phi(x_{ii'}) - \theta^\top y_{ij'})^2 \gamma_{i'j'}^* \right) \\ &= \sum_{i'=1}^{m_{i1}} \sum_{j'=1}^{m_{i2}} \gamma_{i'j'}^* \nabla_\phi (\theta^\top f_\phi(x_{ii'}) - \theta^\top y_{ij'})^2 \\ &= 2 \sum_{i'=1}^{m_{i1}} \sum_{j'=1}^{m_{i2}} \gamma_{i'j'}^* (\theta^\top f_\phi(x_{ii'}) - \theta^\top y_{ij'}) \nabla_\phi (\theta^\top f_\phi(x_{ii'})). \end{aligned} \quad (11)$$

The calculation of $\nabla_{\phi}(\theta^{\top} f_{\phi}(x_{ii'}))$ depends on the form of f_{ϕ} . In the upcoming examples and simulations, we utilize a linear function for simplicity, $f_{A,b}(x) = Ax + b$, i.e., $\phi = (A, b)$ with $A = [A_{ij}] \in \mathbb{R}^{d_2 \times d_1}$ and $b \in \mathbb{R}^{d_2}$. We put a horseshoe prior (Carvalho et al., 2009) on A , which will be later discussed in detail in the context of graph discovery:

$$A_{ij} \mid \lambda_{ij}, \tau \sim \mathcal{N}(0, \lambda_{ij}^2 \tau^2), \quad \lambda_{ij} \sim C^+(0, 1), \quad \tau \sim C^+(0, 1), \quad (12)$$

and $b \sim \mathcal{N}(0, I)$. We implement posterior simulation using standard MCMC transition probabilities using the inverse gamma complete conditional posterior distributions for λ_{ij}^2 , ν_{ij} , τ^2 , and ζ . We refer the reader to Supplementary Materials A for the detail of the MCMC sampler. To sample from $p(A, b \mid \lambda^2, \tau^2, \mathcal{S})$, we use the MALA algorithm as discussed above. Plugging in $\nabla_A(\theta^{\top}(Ax_{ii'} + b)) = \theta x_{ii'}^{\top}$ and $\nabla_b(\theta^{\top}(Ax_{ii'} + b)) = \theta$ into Equation (11), we obtain the gradient for the log-likelihood. For the gradient of the log-prior, we have $\nabla_{A_{ij}} \log p(A_{ij} \mid \lambda_{ij}^2, \tau^2) = \nabla_{A_{ij}} \frac{-A_{ij}^2}{2\lambda_{ij}^2 \tau^2} = \frac{-A_{ij}}{\lambda_{ij}^2 \tau^2}$ and $\nabla_b \log p(b) = \nabla_b \frac{-\|b\|_2^2}{2} = -b$.

3.3 Simulation

We generate distributional samples $\mathcal{S} = \{(F_1, G_1), \dots, (F_N, G_N)\}$ with $N \in \{10, 20, 50, 100, 200\}$.

In particular, letting $A^* = \begin{bmatrix} 1 & 0 \\ 1 & 1 \end{bmatrix}$ and $b^* = [1, 1]^{\top}$, we construct:

$$F_i = \frac{1}{m} \sum_{j=1}^m \delta_{x_{ij}}, \quad G_i = \frac{1}{m} \sum_{j=1}^m \delta_{A^* x_{ij} + b^* + \epsilon_0}$$

where $\epsilon_0 \sim \mathcal{N}([0, 0]^{\top}, I_2)$, and $m = 100$. We consider two simulation scenarios. In scenario 1, we sample $x_{i1}, \dots, x_{im} \stackrel{i.i.d.}{\sim} \mathcal{N}(\mu_i, \Sigma_i)$ with $\mu_i \sim \mathcal{N}([0, 0]^{\top}, 4I_2)$ and $\Sigma_i \sim IW(I_2, 6)$ (inverse Wishart distribution with scale matrix I_2 and degrees of freedom 6) for $i = 1, \dots, N$. Under scenario 2, we sample $x_{i1}, \dots, x_{im} \stackrel{i.i.d.}{\sim} \frac{1}{3}\mathcal{N}(\mu_{i1}, \Sigma_{i1}) + \frac{1}{3}\mathcal{N}(\mu_{i2}, \Sigma_{i2}) +$

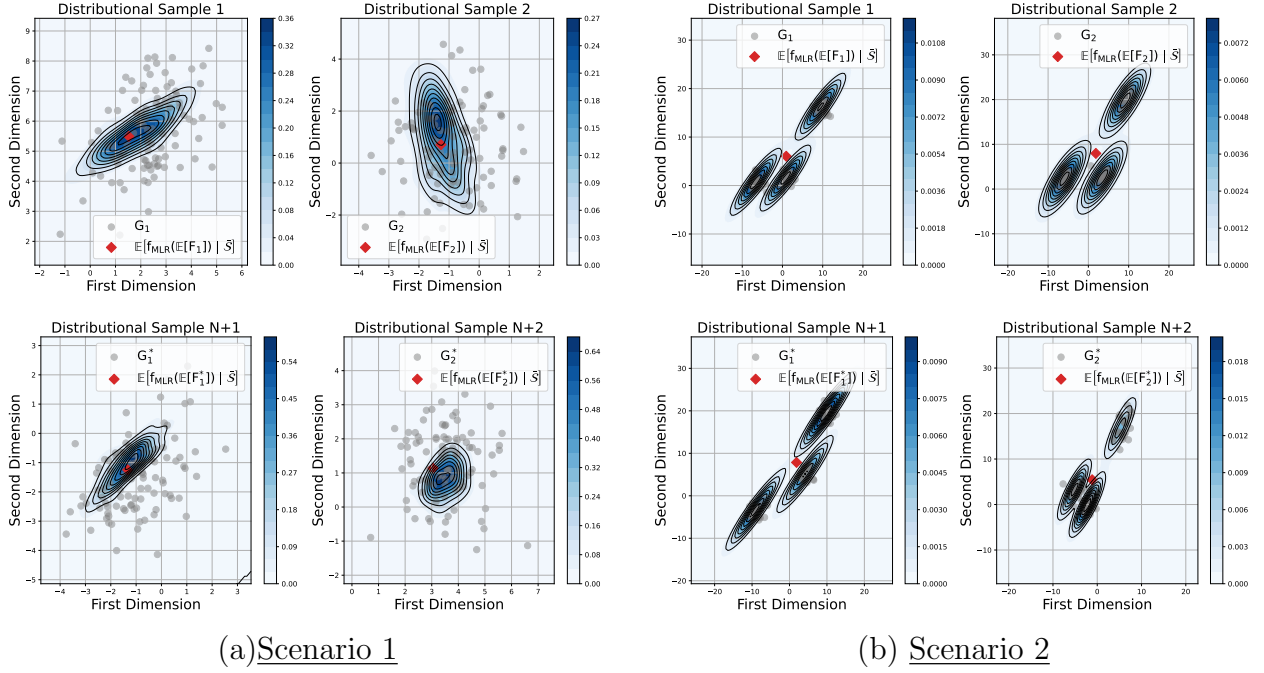


Figure 1: Fitted and predictive densities \bar{G}_i under Bayesian DDR and expected fitted means under Bayesian MLR. The first two columns shows results for two pairs of predictor and response distributions under scenario 1. The last two columns shows the same under scenario 2. The first and second row show fitted (for $i = 1, 2$) and predicted (for $i = N + 1, N + 2$) densities, respectively. Here and in all later figures showing fitted densities \bar{G}_i , the grey dots are the samples from the response distributions, the red diamonds show the fitted mean under Bayesian MLR, and the blue contours are fitted densities under Bayesian DDR.

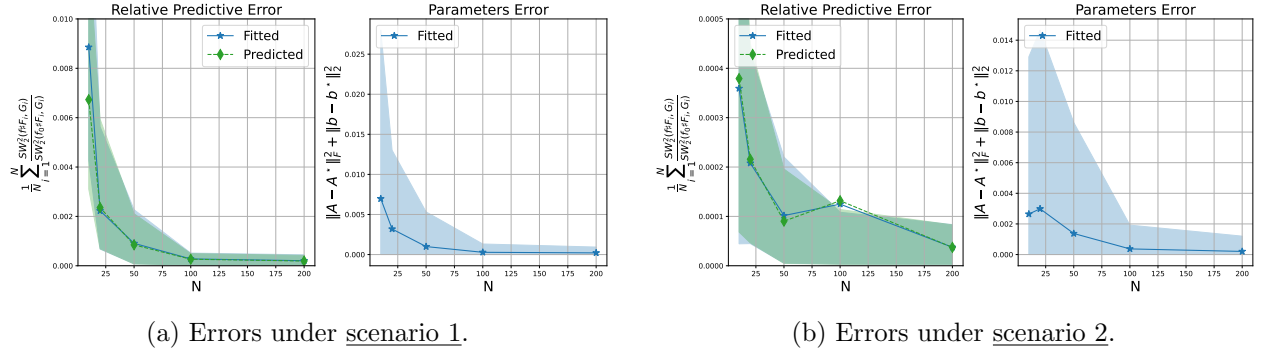


Figure 2: Mean in-sample relative predictive errors (7) (fitted computed with \mathcal{S} and predicted computed with \mathcal{S}^*), and posterior mean squared error $\|A - A^*\|_F^2 + \|b - b^*\|_2^2$ with corresponding 95% credible interval.

$\frac{1}{3}\mathcal{N}(\mu_{i3}, \Sigma_{i3})$, with $\mu_{i1} \sim \mathcal{N}([0, 0]^\top, 4I_2)$, $\mu_{i2} \sim \mathcal{N}([8, 8]^\top, 4I_2)$, $\mu_{i3} \sim \mathcal{N}([-8, 8]^\top, 4I_2)$, and $\Sigma_{i1}, \Sigma_{i2}, \Sigma_{i3} \sim IW(I_2, 6)$ for $i = 1, \dots, N$.

We compare the proposed Bayesian DDR with Bayesian multivariate linear regression (MLR) replacing the distributions G_i and F_i by sample-specific average gene expressions as would be observed in a pseudo-bulk gene expression dataset. That is, the data are

$\bar{\mathcal{S}} = \{(\bar{x}_i, \bar{y}_i)\}$ where $\bar{x}_i = \frac{1}{m_{i1}} \sum_{j=1}^{m_{i1}} x_{ij}$ and $\bar{y}_i = \frac{1}{m_{i2}} \sum_{j=1}^{m_{i2}} y_{ij}$. Let $\bar{X} = (\bar{x}_1, \dots, \bar{x}_N)$ and $\bar{Y} = (\bar{y}_1, \dots, \bar{y}_N)$. The Bayesian MLR model is

$$\bar{Y} \mid \bar{X}, A, \Sigma \sim \mathcal{MN}(\bar{X}A, \Sigma, I), \quad A \mid \Sigma \sim \mathcal{MN}(0, \Sigma, I), \quad \Sigma \sim IW(I, d_2). \quad (13)$$

where $\mathcal{MN}(M, U, V)$ denotes the matrix normal distribution with location matrix M and scale matrices U and V , and the intercepts are included in A . Inference under the Bayesian MLR model is implemented by a Gibbs sampler alternating draws from the complete conditional posterior distributions for A and Σ :

$$\Sigma \mid \bar{Y}, \bar{X}, A \sim IW(V_N, \nu_N), \quad A \mid \bar{Y}, \bar{X}, \Sigma \sim \mathcal{MN}(B_N, \Lambda_N^{-1}, \Sigma)$$

with $V_N = I + (\bar{Y} - \bar{X}A)^\top (\bar{Y} - \bar{X}A) + (A - A_0)^\top (A - A_0)$, $B_N = (\bar{X}^\top \bar{X} + I)^{-1} (\bar{X}^\top \bar{Y} + A_0)$, $\Lambda_N = \bar{X}^\top \bar{X} + I$, and $\nu_N = d_2 + N$.

For both, Bayesian DDR and Bayesian MLR, we save 1000 MCMC samples. For the MALA algorithm of Bayesian DDR, we use a step size $\eta = 10^{-5}$, and we use $w = 10$ in the generalized likelihood. We discard the first 500 samples as burn-in samples. With the final $T = 500$ posterior samples $\{A_1, \dots, A_T; b_1, \dots, b_T\}$ we evaluate distributional predictions $\bar{G}(z)$ for any predictor distribution $F = \frac{1}{m} \sum_{i=1}^m \delta_{x_i}$ as $\bar{G}(z) = \mathbb{E}[(f_{A,b}^\# F)(z) \mid \mathcal{S}]$.

In the first row of Figure 1 we visualize the fitted densities (i.e., in-sample prediction) \bar{G} under the Bayesian DDR and the fitted means under MLR for 2 randomly chosen distributional samples under both scenarios, with $N = 10$. Here and in later figures we use kernel density estimation to smooth the shown contours. Inference under the Bayesian DDR reports distributions whereas inference under the Bayesian MLR yields a single vector. For the mixture of Gaussians case (scenario 2), the expected means under the Bayesian MLR

are not even in a high probability region.

For an assessment of inference as a function of sample size, we evaluate the change in RPE and the change in posterior expected squared error for parameters, $\|A - A^*\|_F^2 + \|b - b^*\|_2^2$, as functions of sample size N . Results are shown in Figure 2. To compute RPE, we define the reference model f_0 in (7) as intercept model, with $A = 0$, leaving only the intercept b . From Figure 2, we see that both, RPE (in blue) and parameters mean squared error decrease with N as expected. From this simulation, we observe that the generalized posterior under Bayesian DDR already concentrates around the true parameters for theoretically feasible sample sizes N .

Next, we consider out-of-sample prediction. We use a test sample $\mathcal{S}^* = \{(F_{N+1}, G_{N+1}), \dots, (F_{N+N^*}, G_{N+N^*})\}$, which are generated under the same simulation truths (scenarios 1 and 2) as before. We use $N^* = 200$ (the large N^* is needed for the evaluation of $\overline{\text{RPE}}$). The second row of Figure 1 shows out-of-sample predicted densities $\bar{G}_i(z) = \mathbb{E}[(f_{A,b} \# F_i)(z) \mid \mathcal{S}]$ for two randomly chosen distributional samples in the test set, conditional on a training sample of size $N = 10$, under both scenarios. Predictive inference under the Bayesian DDR matches the observed densities quite well, confirming the desired generalizability. We further evaluate generalizability by evaluating out-of-sample RPE in Figure 2 in green color. Again, we find decreasing out-of-sample RPE with increasing sample size, as expected.

4 Example: Cell to Cell Communication

Cell-cell communication plays a fundamental role in understanding complex biological systems, as interactions between cells drive various physiological and pathological processes. A natural way to quantify these interactions is by modeling how the distribution of ligands of one cell type influences the distribution of receptors of another cell type. We demonstrate

the proposed generalized Bayesian DDR with an application to inference on the communication between B cells and T cells using the population-scale single-cell data, OneK1K (Yazar et al., 2022). We select 439 donors who have at least 100 observed cells for both cell types. We formalize cell to cell communication as a regression of a distribution of gene expressions of T cell receptors (as response) on gene expression of B cell ligands (as predictor) to represent “B cell to T cell” communication, and vice versa for “T cell to B cell.” Letting G_i denote the distribution of T cell receptor gene expression for sample i (as empirical distribution), and F_i the same for B cell ligands, the regression of T cell on B cell gene expression becomes a density-density regression as in (5) for the pairs (F_i, G_i) . And similarly for T to B. For the regression of T cell gene expression on B cell gene expression (B cells to T cells) the predictor is the distribution F_i of B cell ligands {CD40, CD86, ICOSL, IL-6, BAFF, APRIL} and the response is the distribution G_i of T cell receptors {CD3D, CD3E, CD3G, TRBC1, TRBC2, CD28, ICOS, IL-2R, IFNGR, IL-21R, PD-1, CTLA-4, CXCR5, CCR7}. For T cells to B cells, the predictor is the distribution of T cell ligands {CD40L, IFN- γ } and the response is the distribution of B cell receptors {IGHM, IGHD, IGHG, IGHA, CD40, ICOSL, IL-21R, IL-6R, BAFFR, CXCR5, CCR7}. The orthogonal nature of the ligand and receptor sets makes the regressions of T on B and B on T complementary. For each task, we split the set of donors into a training set with 80% of the subjects and a test set with the remaining 20%. We standardize all ligands and receptors based on the mean and standard deviation from all cells and all donors in the training set.

For the MALA algorithm, we use a step size $\eta = 10^{-4}$. In the definition of the generalized log-likelihood, we use a factor $w = 100$, and we use $L = 1000$ for approximating the SW distance. We obtain 1000 MCMC samples and discard the first 500 samples for both the Bayesian DDR and the Bayesian MLR. Figure 3 shows the fitted densities \bar{G} of 4

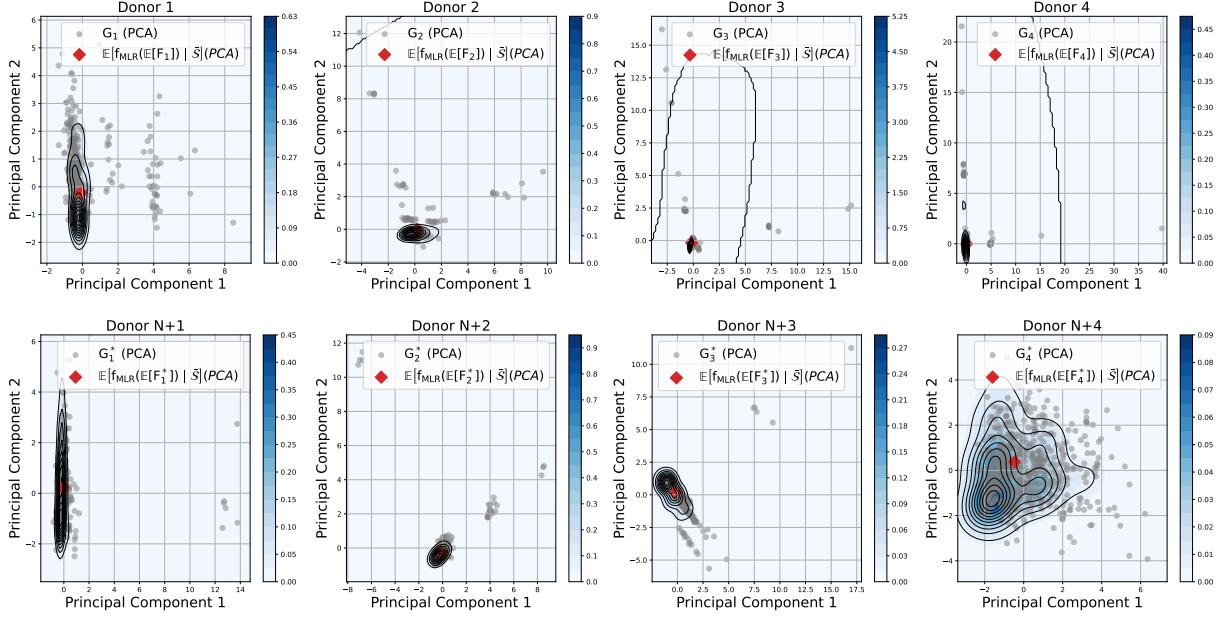


Figure 3: Density-density regression of T cell gene expression on B cell gene expression under the Bayesian DDR model. The first row shows posterior fitted densities \bar{G}_i for four randomly chosen samples in the training set (in-sample). The second row shows predictive densities \bar{G}_i for four randomly chosen samples in the test set (out-of-sample). Compare with Figure 1 for an explanation of the symbols and contours. Here and in all later figures illustrating high dimensional gene expression features, we use PCA on the atoms of the observed response distribution for each donor to plot the first two projections.

randomly selected donors in the training set (first row of panels) and the predicted densities \bar{G} for 4 random donors in the test set (second row of panels) under the proposed Bayesian DDR of T cell gene expression on B cell gene expression. For comparison, we also indicate the fitted and predicted values for \bar{y}_i under the Bayesian MLR. For the Bayesian DDR, we show contour plots of fitted and predicted $\bar{G} = \mathbb{E}[(f_{A,b} \# F) \mid F, \mathcal{S}]$ for predictor $F_i = F$.

For each donor, we plot the first two projections under PCA of the atoms of the observed response distribution G_i . As a density-density regression, Bayesian DDR reports an entire distribution, while Bayesian MLR naturally only reports a single point estimate of \bar{y}_i . We use RPEs as defined in (7) to assess the fit and prediction. For the regression of T cell gene expression on B cell gene expression shown in Figure 3, under the Bayesian DDR we find posterior mean RPEs of 0.233 with a 95% credible interval of [0.232, 0.235] for the fitted densities in the training set, and 0.217 (0.216 to 0.219) for the predicted densities

for the test set. For the regression of B cell gene expression on T cell gene expression (not shown), we find the posterior mean RPE of 0.617 (0.616 to 0.619) for the training set and 0.606 (0.603 to 0.609) for the test set.

In summary, T cell receptor expression can be fitted well using $f_{A,b} \sharp F_i$, via the linear mapping $f_{A,b}$, while the distribution of B cell receptor expression can be partially linearly explained by T cell ligand expression.

5 Application to Graph Discovery

We extend DDR to a setting with multiple pairs of distributions. The goal is to discover a directed network or graph of these distributions. A directed graph is a pair $\mathcal{G} = (\mathcal{V}, \mathcal{E})$ where $\mathcal{V} = \{v_1, \dots, v_V\}$ is a set of nodes and $\mathcal{E} \subseteq \mathcal{E}_0 = \{(\ell, r) \mid \ell, r \in \mathcal{V}, \ell \neq r\}$ is a set of directed edges. For each pair $e = (\ell, r) \in \mathcal{E}_0$, we observe a sample of N_e pairs of distributions $\mathcal{S}_e = \{(F_{ei}, G_{ei})\}_{i=1}^{N_e}$. We introduce two approaches to discover a directed graph of distributional nodes. The first option is to report a fully connected graph with edges labeled by weights generated from DDR. The second approach casts the graph discovery as a decision problem, which we address by way of a simple decision boundaries. In both cases, the graph is reported as a posterior summary based on the generalized posterior (8).

To define a **weighted fully connected graphs** we start by setting up a Bayesian DDR model for each edge $e \in \mathcal{E}_0$. Using inference under the DDR model, we evaluate the relative predictive error as defined in (6),

$$RPE_e(\mathcal{S}_e, L) = \frac{1}{N_e} \sum_{i=1}^{N_e} \frac{\widehat{SW}_2^2(f_e \sharp F_{ei}, G_{ei}; L)}{\widehat{SW}_2^2(f_{e0} \sharp F_{ei}, G_{ei}; L)}, \quad (14)$$

which is estimated as

$$\overline{\text{RPE}}_e(\mathcal{S}_e, L) = \frac{1}{T} \frac{1}{N_e} \sum_{t=1}^T \sum_{i=1}^{N_e} \frac{\widehat{SW}_2^2(f_{et} \# F_{ei}, G_{ei}; L)}{\widehat{SW}_2^2(f_{e0t} \# F_{ei}, G_{ei}; L)}, \quad (15)$$

using posterior samples $f_{e1}, \dots, f_{eT} \sim p(f_e \mid \mathcal{S}_e)$ and $f_{e01}, \dots, f_{e0T} \sim p(f_{e0} \mid \mathcal{S}_e)$ under a reference model f_{e0} . For example, if f_e is a linear mapping, as we shall use it later, the reference model f_{e0} is the intercept model. Given the posterior mean RPE for all pairs, we report a fully connected graph with the estimated RPEs as weights for directed edges.

For an alternative approach, we define a **sparse graph based on FDR and FNR control**. We augment the inference model to a decision problem by adding a loss function. First, we use a linear mapping $f_{A,b}(x) = Ax + b$ with parameters $\phi = (A, b)$. We place the horseshoe prior on A , as before, in (12). Let A_e be the linear coefficient matrix in $f_{A,b}$ that maps from F_{ei} to G_{ei} for $i = 1, \dots, N_e$. We define the ϵ -inclusion probability ($\epsilon > 0$):

$$p_e = \mathbb{P}\left(\max_{ij} \{|A_{eij}|\} > \epsilon \mid \mathcal{S}_e\right) \quad i = 1, \dots, d_{e1}; j = 1, \dots, d_{e2}, \quad (16)$$

where d_{e1} and d_{e2} are the dimensions of \hat{G}_{ei} and \hat{F}_{ei} . The probability can be estimated using the MCMC samples for A_e . We interpret the event $\max_{ij} \{|A_{eij}|\} > \epsilon$ as the presence of edge e , and use p_e to define a parametrized decision rule. We include edge $e = (\ell, r)$ if $p_e > 0.5$. that is, we use the rule $\tilde{d}_e = I(p_e > 0.5)$. The rule \tilde{d}_e reduces the decision to the choice of a single decision parameter ϵ . We use a loss function based on posterior expected false discovery rate ($\overline{\text{FDR}}$) and false negative rate ($\overline{\text{FNR}}$) to choose ϵ . In short, for a fixed bound on $\overline{\text{FDR}}$, we choose ϵ to minimize $\overline{\text{FNR}}$. The two error rates are defined as

$$\overline{\text{FDR}} = \frac{\sum_{e \in \mathcal{E}_0} (1 - p_e) \tilde{d}_e}{\sum_{e \in \mathcal{E}_0} \tilde{d}_e + 0.001} \quad \text{and} \quad \overline{\text{FNR}} = \frac{\sum_{e \in \mathcal{E}_0} p_e (1 - \tilde{d}_e)}{|\mathcal{E}_0| - \sum_{e \in \mathcal{E}_0} \tilde{d}_e + 0.001}, \quad (17)$$

Ordered Pairs	N	Ligands F_i	Receptors G_i
T Cells to B Cells	439	CD40L, IFN- γ	IGHM, IGHD, IGHG, IGHA, CD40, ICOSL, IL-21R, IL-6R, BAFFR, CXCR5, CCR7
B Cells to T Cells	439	CD40, CD86, ICOSL, IL-6, BAFF, APRIL	CD3D, CD3E, CD3G, TRBC1, TRBC2, CD28, ICOS, IL-2R, IFNGR, IL-21R, PD-1, CTLA-4, CXCR5, CCR7
T Cells to monocytes	130	CD40L, IFN- γ , CD70	CD86, IL-12R, TNFR1, TNFR2, IL-6R, CXCR4, PD-1, LAG-3
monocytes to T Cells	130	CD86, ICOSL, IL-23, TNF- α , IL-1 β , IL-6, CD70	CD3D, CD3E, CD3G, TRBC1, TRBC2, CD28, ICOS, IL-2R, IFNGR, IL-21R, PD-1, CTLA-4, CXCR3, CXCR4
B Cells to monocytes	59	CD40L, CD70, IL-6, TNF- α , Tim-3, BAFF, APRIL	CD40, CD86, IL-12R, TNFR1, TNFR2, CXCR3, PD-1, LAG-3
monocytes to B Cells	59	CD40L, IL-6, TNF- α , Tim-3, BAFF, APRIL	CD40, IL-6R, IL-10R, BAFF-R, CXCR4, CCR7, PD-1
monocytes to NK Cells	102	CD40L, TNF- α , IL-15, IL-18, Tim-3	NKG2D, NKp30, NKp46, DNAM-1, NKG2A, IL-2R, IL-15R
NK Cells to monocytes	102	IL-15, IFN- γ , FasL	IL-12R, IL-15R, IFN- γ R, CXCR3, Fas, CD40, PD-1, Tim-3
NK Cells to T Cells	700	IL-15, IFN- γ , CD40L, FasL	IL-12R, IL-15R, IFN- γ R, CD28, ICOS, PD-1, Tim-3
T Cells to NK Cells	700	IFN- γ , CD86	IL-2R, IL-4R, IL-21R, IFN- γ R, CCR1, CXCR3, CD28, ICOS, PD-1, Tim-3, NKG2D
B Cells to NK Cells	319	IL-6, BAFF, TNF- α , CD40L	IL-6R, BAFF-R, TNFR, IL-10R, CCR1, CXCR3, CD40, ICOS, PD-1, Tim-3, NKG2D
NK Cells to B Cells	319	IL-15, IFN- γ , CXCL8, CD40L	IL-2R, IL-15R, IFN- γ R, CCR1, CXCR2, CD40, ICOS, PD-1, Tim-3

Table 1: Summary of a dataset of 4 cell types: B cells, T cells, and NK cells, and monocytes. For each pair the table lists the number of donors and the list of ligands and receptors.

where $|\mathcal{E}_0|$ is the total number of possible edges (and 0.001 in the denominator avoids 0-denominators). See, for example, Müller et al. (2004) for a discussion of $\overline{\text{FDR}}$ and $\overline{\text{FNR}}$.

We choose ϵ to minimize $\overline{\text{FNR}}$ subject to $\overline{\text{FDR}} \leq 0.10$.

6 Example: A Cell-Cell Communication Graph

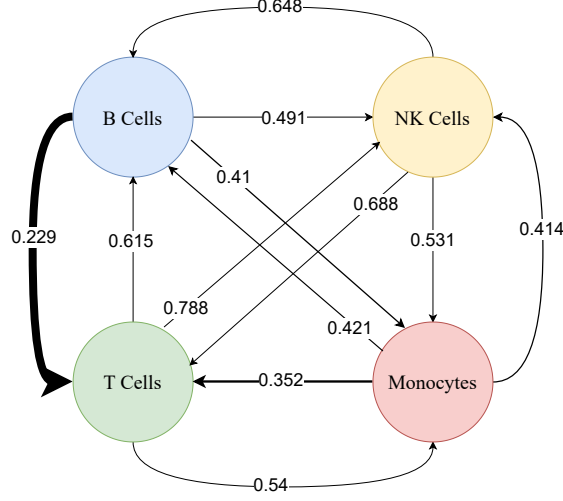
6.1 Results for the OneK1K single-cell data

We consider four cell types from the OneK1K dataset: B cells, T cells, NK cells, and monocytes, and aim to infer a graph to represent cell-cell communication between these

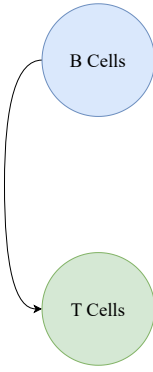
four subtypes. For each ordered pair of cell types, we extract the ligand genes from the “sender” cell and the receptor genes from the “receiver” cell and regress the distribution of gene expression for the latter onto the distribution of the former. The data are the observed distributions of single-cell RNA-seq gene expression for donors $i = 1, \dots, N$. We select only donors who have at least 100 cells. Table 1 shows the number of donors N for each ordered pair of cell types and the list of ligands and receptors. We standardize all ligands and receptors across all cells and donors. We implement Bayesian DDR using a linear function $f_{A,b}(x) = Ax + b$ and Bayesian MLR. Under both models, we generate 1000 MCMC samples with the first 500 samples discarded as burn-in. We use a step size of $\eta = 10^{-4}$ for the MALA algorithm, and a scale factor of $w = 100$ in the generalized log-likelihood function.

As before, for visualization we use PCA on the response distribution of each donor to obtain the projection matrix in two dimensions. Figures 7-10 in Supplementary Materials B shows fitted densities \bar{G} under Bayesian DDR for ordered pairs of cell types. For comparison, as before, we also include fitted means under Bayesian MLR. Bayesian DDR reports entire fitted densities \bar{G} . In contrast, Bayesian MLR provides a single fitted value for \bar{y} , stopping short of representing the entire distributional information of the response.

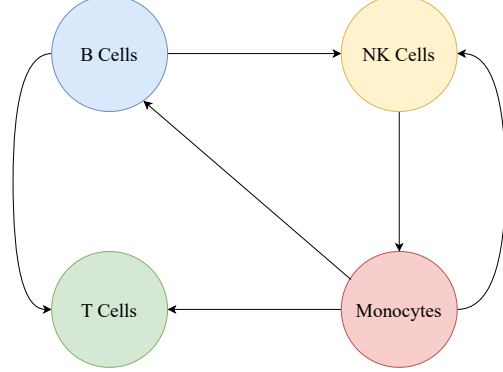
Figure 4a shows an estimated graph of cell-cell communication, with edge weights based on mean RPE. Lower mean RPE means a higher level of association. We use an exponential kernel based on mean RPE to control the thickness of the edges. We refer the reader to Figure 8 in Supplemental Materials B for boxplots of RPE for all ordered pairs of cell types. For an alternative graph estimate, we show in Figure 4b and Figure 4c the graph based on FDR and FNR control as discussed before. For comparison, we also report an estimated graph based on inference under Bayesian MLR (using the same FDR and FNR



(a) Graph discovered by RPEs (7)



(b) Graph discovered by MLR



(c) Graph discovered by DDR

Figure 4: (a) Weighted graph using mean RPE under the Bayesian DDR model. Edge thickness is controlled by an exponential kernel of mean RPE, showing thicker edges for lower mean RPE. Estimated graphs under (b) Bayesian MLR and, (c) Bayesian DDR. Both are based on FDR and FNR control.

control). For Bayesian MLR, we found the optimal threshold $\epsilon = 0.858$, yielding posterior expected FDR and FNR of $(\overline{\text{FDR}}, \overline{\text{FNR}}) = (0.1, 0.039)$. Under the Bayesian DDR, the optimal threshold is $\epsilon = 0.974$, corresponding to $\overline{\text{FDR}} = 0.1, \overline{\text{FNR}} = 0.108$. The graph based on Bayesian MLR includes only one edge from B to T cells. Under the Bayesian DDR model we find 6 edges: B to T cells, B to NK cells, monocytes to T cells, monocytes to NK cells, NK cells to monocytes, and monocytes to B cells. Comparing with the mean RPE weights in Figure 4a, we note that the estimated graph under FDR and FNR control

seems to select edges with the mean RPE smaller than 0.5.

Besides facilitating the graph construction, another benefit of choosing the linear function $f_{A,b}$ is the opportunity to explore the interaction between ligands and receptors through inference on the corresponding coefficients in A . Figures 11-22 in Supplementary Materials B show boxplots for the linear regression coefficients A for all ordered pairs of cell types. From these summaries, one could determine which ligands are significant in predicting specific receptors. We discuss more details in the Supplementary Materials B.

6.2 Semi-Simulation

We validate the proposed graph discovery framework by setting up a simulation using simulation truths inspired by the OneK1K data. Particularly, we use the real predictor distributions taken from the data and a simulation truth for $f_{A,b}$ estimated from the real data to set up a simulation truth for the response distributions. Assume then from the earlier data analysis we have a posterior Monte Carlo sample with T posterior samples under the Bayesian DDR model for all pairs of cell types. Recall that $\tilde{d}_e \in \{0, 1\}$ is an indicator for including edge e in the inferred graph under Bayesian DDR (Figure 4c). We define the following empirical distributions:

$$p_1 \propto \sum_{e \in \mathcal{E}_0} \sum_{t=1}^T \sum_{i=1}^{d_{e1}} \sum_{j=1}^{d_{e2}} \delta_{A_{eijt}} I(\tilde{d}_e = 1) \text{ and } p_0 \propto \sum_{e \in \mathcal{E}_0} \sum_{t=1}^T \sum_{i=1}^{d_{e1}} \sum_{j=1}^{d_{e2}} \delta_{A_{eijt}} I(\tilde{d}_e = 0),$$

where A_{eijt} is the (i, j) element of A_e in the t -th MCMC sample for cell types $e = (\ell, r)$. That is, p_1 is the empirical distribution of coefficients for included edges in Figure 4b, and p_0 is the same for missing edges. We consider the following three scenarios: Under scenario 1 (“no edge”) we sample for each pair $e = (\ell, r)$ of cell types the simulation truth $A_{eij}^* \sim p_0$ and $b_{ej}^* \sim p_0$ ($i = 1, \dots, d_{e1}$, $j = 1, \dots, d_{e2}$). Under scenario 2 (“full

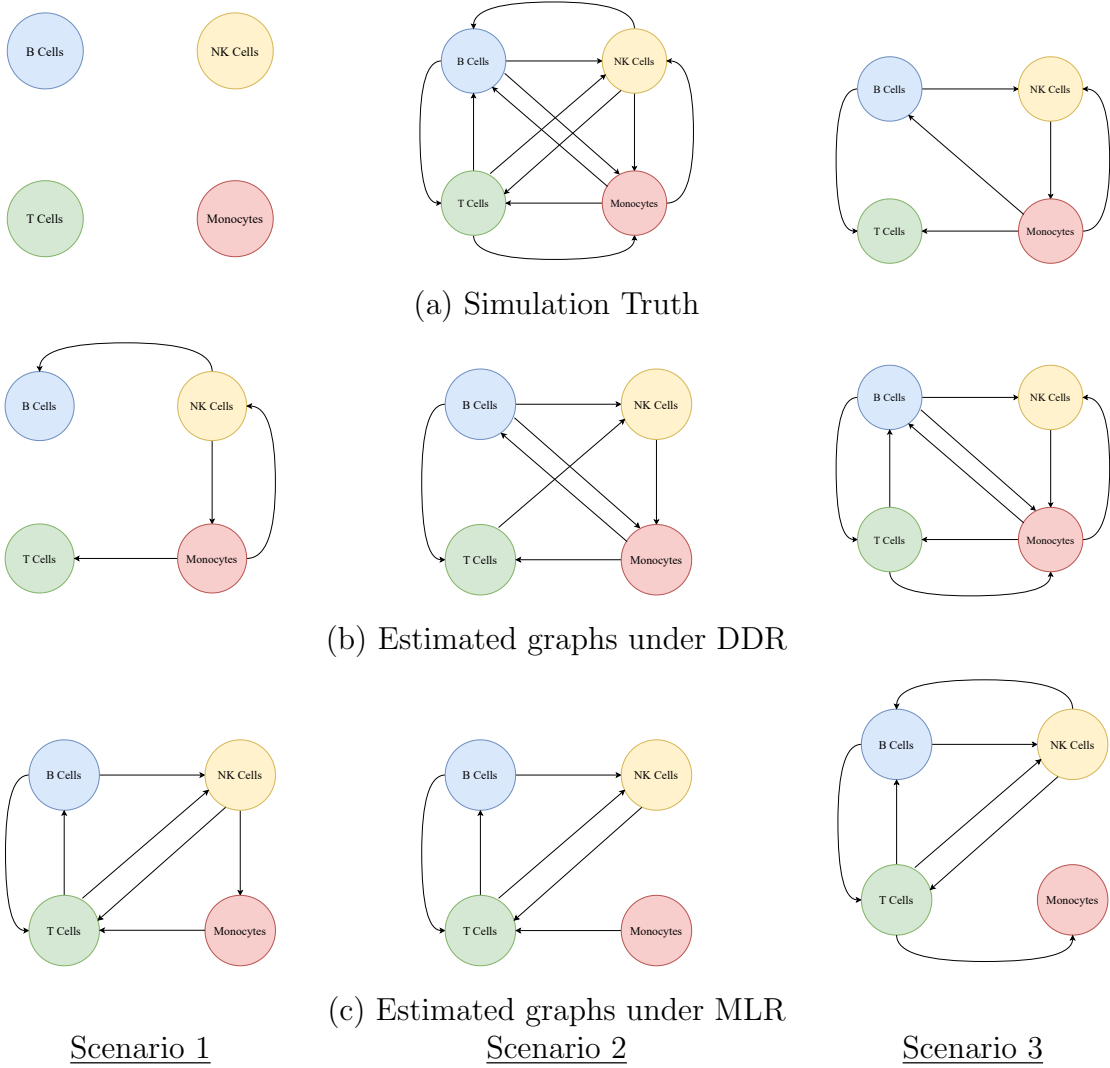


Figure 5: Simulated true graphs (first row) and estimated graphs under the Bayesian DDR model (second row) and the Bayesian MLR model (third row) using FDR and FNR control in the “no edge”-scenario 1 (left column), “full graph”-scenario 2 (center column), and “sparse graph” -scenario 3 (right column) scenarios.

graph”) we sample the simulation truth for all pairs $e = (\ell, r)$ as $A_{eij}^* \sim p_1$ and $b_{ej}^* \sim p_1$ ($i = 1, \dots, d_{e1}$), $j = 1, \dots, d_{e2}$). Finally, under scenario 3 (“sparse graph”) we use the inferred graph under Bayesian DDR (Figure 4b) as the ground truth. For included edges e , we sample the simulation truth like under scenario 2. For excluded edges we sample like under scenario 1. Under all three scenarios, after generating the simulation truths (A_e, b_e) for the linear mappings, we simulate response distributions $G_{ei} = \frac{1}{m_{ei}} \sum_{j=1}^{m_{ei}} \delta_{A_e^* x_{ij} + b_e^* + \epsilon_0}$ where x_{ij} is the observed ligands gene expression from the i -th donor in the OneK1K data,

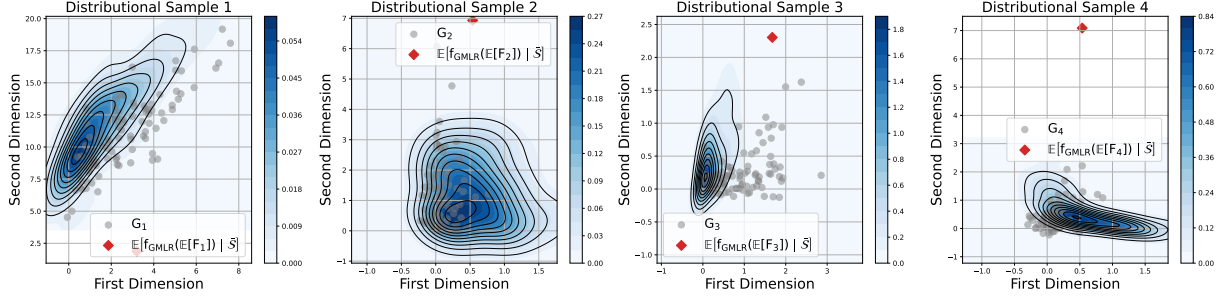


Figure 6: Fitted densities \bar{G} under Bayesian DDR with quadratic mapping $f_{A,b}$ fitted means under a Bayesian multivariate nonlinear regression, with quadratic mean function.

and $\epsilon_0 \sim \mathcal{N}(0, 0.01I)$ for $i = 1, \dots, N_e$. This concludes the definition of the simulation truth. We then implement inference under the Bayesian DDR and the Bayesian MLR model, with the same hyperparameters as in the earlier data analysis. We then use FDR and FNR control to report a graph.

Inference under Bayesian DDR. Figure 5 shows the simulated true graphs and the reported graphs under the Bayesian DDR model for all three scenarios. Under scenario 1 (“no edge”) we find the optimal threshold as $\epsilon = 1$, yielding $(\overline{\text{FDR}}, \overline{\text{FNR}}) = (0.035, 0.064)$, and 5 edges are found. Under scenario 2 (“full graph”), $\epsilon = 1$ with $(\overline{\text{FDR}}, \overline{\text{FNR}}) = (0.083, 0.125)$, and 7 edges are discovered. Finally, under scenario 3 (“sparse graph”), $\epsilon = 1$, and $(\overline{\text{FDR}}, \overline{\text{FNR}}) = (0.036, 0.17)$. In this setup, Bayesian DDR yields 9 edges, with 6 correct edges and 3 incorrect edges. Boxplots of RPE for all ordered pairs of cell types, and under all three scenarios is shown in in Figure 23 in Supplementary Materials C. The relatively low RPE values show a good fit for almost all ordered pairs of cell types across all three settings. Additionally, Figure 24 in Supplementary Materials C shows boxplots of squared errors for the parameters (A_e, b_e) for the three settings and all pairs of cell types. Overall we find relatively small parameter errors in all cases.

Inference under Bayesian MLR: Note that under all three scenarios the simulation truth is based on a linear mapping of the atoms in F_i , implying a linear relationship also

between $\bar{x}_i = \frac{1}{m_{i1}} \sum_{j=1}^{m_{i1}} x_{ij}$ and $\bar{y}_i = \frac{1}{m_{i2}} \sum_{j=1}^{m_{i2}} y_{ij}$. Those are the measurements reported by experimental platforms that record bulk gene expression in samples. Naturally, this setting favors Bayesian MLR, which yields the following $(\overline{\text{FDR}}, \overline{\text{FNR}})$ values: (0.083, 0.007) for scenario 1 (“no edge”); (0.007, 0.008) for scenario 2 (“full graph”); and (0.071, 0.039) for scenario 3 (“sparse graph”). The estimated graphs are shown in Figure 5. In all three cases, the FNR under DDR was higher, but remained within practically useful bounds.

The previous simulation included a linear (in the atoms) simulation truth, favoring MLR (since it also implies linearity of mean bulk gene expression). To highlight the limitations of linear regression for bulk gene expression (\bar{x}, \bar{y}) we consider another simulation, with: $F_i = \frac{1}{m} \sum_{j=1}^m \delta_{x_{ij}}$, $G_i = \frac{1}{m} \sum_{j=1}^m \delta_{(A^* x_{ij} + b^*)^2 + \epsilon_0}$, where $A^* = \begin{bmatrix} 1 & 0 \\ 1 & 1 \end{bmatrix}$, $b^* = [1, 1]'$, $\epsilon_0 \sim \mathcal{N}([0, 0]', 0.01I)$, and $m = 100$. We sample $x_{i1}, \dots, x_{im} \stackrel{i.i.d.}{\sim} \mathcal{N}(\mu_i, \Sigma_i)$ with $\mu_i \sim \mathcal{N}([0, 0]', I)$ and $\Sigma_i \sim IW(10, I)$ for $i = 1, \dots, N = 10$. We implement Bayesian DDR with $f_{A,b}(x) = (Ax + b)^2$ (element-wise quadratic), and compare with inference under a Bayesian multiple nonlinear regression (MNR) assuming $\bar{y} \mid \bar{x}, A, \Sigma \sim \mathcal{MN}((\bar{x}A)^2, \Sigma, I)$ (element-wise quadratic). Figure 6 shows the fitted densities under Bayesian DDR and fitted means under the Bayesian MNR model. While inference under the Bayesian DDR can still capture the high-density regions, Bayesian MNR naturally gives inaccurate fits of the mean, due to model mis-specification. Similarly, in cases where $\mathbb{E}[X_i] = 0$ or $\mathbb{E}[X_i]$ does not exist (e.g., Cauchy distribution), Bayesian MLR based on the mean statistic is not feasible, while Bayesian DDR remains well-defined.

7 Conclusion

We introduced Bayesian Density-Density Regression (Bayesian DDR) as a novel framework for modeling complex regression relationships between multivariate random distributions.

Some limitations remain. First, the framework can suffer from model misspecification due to the use of the parametric mapping f_ϕ . However, in simulations and in the application we found it sufficiently flexible. The MALA sampling algorithm may not be optimal for ensuring a well mixing Markov chain, due to the non-convex nature of sliced Wasserstein (Tanguy et al., 2025). Moreover, using the conventional sliced Wasserstein distance for generalized likelihood might not be suitable for all types of distributions with non-Euclidean structures. For the graph discovery framework, the ϵ -inclusion probability is an ad-hoc choice, allowing many alternatives.

Future work will focus on addressing these limitations. For instance, we may extend the framework to Bayesian nonparametric density-density regression. In contrast to recent frequentist nonparametric density-density regression approaches (Chen et al., 2023; Ghodrati and Panaretos, 2022), which focus on one-dimensional regression, we envision a Bayesian nonparametric prior for the regression function in multivariate settings. Finally, one could explore alternative geometric variants of the SW distance for the generalized likelihood, and other loss functions or policies for graph discovery.

SUPPLEMENTARY MATERIALS

The Supplementary Materials include additional materials and visualizations, as mentioned in the main text.

References

- Bissiri, P. G., Holmes, C. C., and Walker, S. G. (2016). A general framework for updating belief distributions. *Journal of the Royal Statistical Society Series B: Statistical Methodology*, 78(5):1103–1130.

- Boedihardjo, M. T. (2025). Sharp bounds for max-sliced Wasserstein distances. *Foundations of Computational Mathematics*, pages 1–32.
- Bonneel, N., Rabin, J., Peyré, G., and Pfister, H. (2015). Sliced and Radon Wasserstein barycenters of measures. *Journal of Mathematical Imaging and Vision*, 1(51):22–45.
- Carvalho, C. M., Polson, N. G., and Scott, J. G. (2009). Handling sparsity via the horseshoe. In *Artificial Intelligence and Statistics*, pages 73–80. PMLR.
- Chen, Y., Lin, Z., and Müller, H.-G. (2023). Wasserstein regression. *Journal of the American Statistical Association*, 118(542):869–882.
- Dunson, D. B., Pillai, N., and Park, J.-H. (2007). Bayesian density regression. *Journal of the Royal Statistical Society Series B: Statistical Methodology*, 69(2):163–183.
- Fournier, N. and Guillin, A. (2015). On the rate of convergence in Wasserstein distance of the empirical measure. *Probability theory and related fields*, 162(3):707–738.
- Ghodrati, L. and Panaretos, V. M. (2022). Distribution-on-distribution regression via optimal transport maps. *Biometrika*, 109(4):957–974.
- Girolami, M. and Calderhead, B. (2011). Riemann manifold Langevin and Hamiltonian Monte Carlo methods. *Journal of the Royal Statistical Society Series B: Statistical Methodology*, 73(2):123–214.
- Kolouri, S., Nadjahi, K., Simsekli, U., Badeau, R., and Rohde, G. (2019). Generalized sliced Wasserstein distances. In *Advances in Neural Information Processing Systems*, pages 261–272.
- Leluc, R., Dieuleveut, A., Portier, F., Segers, J., and Zhuman, A. (2024). Sliced-wasserstein

- estimation with spherical harmonics as control variates. In *International Conference on Machine Learning*, pages 27191–27214. PMLR.
- Matabuena, M. and Petersen, A. (2023). Distributional data analysis of accelerometer data from the NHANES database using nonparametric survey regression models. *Journal of the Royal Statistical Society Series C: Applied Statistics*, 72(2):294–313.
- Müller, P., Parmigiani, G., Robert, C., and Rousseau, J. (2004). Optimal sample size for multiple testing: the case of gene expression microarrays. *Journal of the American Statistical Association*, 99(468):990–1001.
- Nadjahi, K., Durmus, A., Chizat, L., Kolouri, S., Shahrampour, S., and Simsekli, U. (2020). Statistical and topological properties of sliced probability divergences. *Advances in Neural Information Processing Systems*, 33:20802–20812.
- Nguyen, K., Bariletto, N., and Ho, N. (2024). Quasi-monte carlo for 3d sliced Wasserstein. In *The Twelfth International Conference on Learning Representations*.
- Nguyen, K. and Ho, N. (2024). Sliced Wasserstein estimator with control variates. *International Conference on Learning Representations*.
- Nguyen, K., Ho, N., Pham, T., and Bui, H. (2021). Distributional sliced-Wasserstein and applications to generative modeling. In *International Conference on Learning Representations*.
- Nietert, S., Goldfeld, Z., Sadhu, R., and Kato, K. (2022). Statistical, robustness, and computational guarantees for sliced wasserstein distances. *Advances in Neural Information Processing Systems*, 35:28179–28193.

- Peyré, G., Cuturi, M., et al. (2019). Computational optimal transport: With applications to data science. *Foundations and Trends in Machine Learning*, 11(5-6):355–607.
- Póczos, B., Singh, A., Rinaldo, A., and Wasserman, L. (2013). Distribution-free distribution regression. In *artificial intelligence and statistics*, pages 507–515. PMLR.
- Rabin, J., Ferradans, S., and Papadakis, N. (2014). Adaptive color transfer with relaxed optimal transport. In *2014 IEEE International Conference on Image Processing (ICIP)*, pages 4852–4856. IEEE.
- Rabin, J., Peyré, G., Delon, J., and Bernot, M. (2012). Wasserstein barycenter and its application to texture mixing. In *Scale Space and Variational Methods in Computer Vision: Third International Conference, SSVM 2011, Ein-Gedi, Israel, May 29–June 2, 2011, Revised Selected Papers 3*, pages 435–446. Springer.
- Shen, W. and Ghosal, S. (2016). Adaptive bayesian density regression for high-dimensional data. *Bernoulli*, pages 396–420.
- Sisouk, K., Delon, J., and Tierny, J. (2025). A user guide to sampling strategies for sliced optimal transport. *arXiv preprint arXiv:2502.02275*.
- Szabó, Z., Sriperumbudur, B. K., Póczos, B., and Gretton, A. (2016). Learning theory for distribution regression. *Journal of Machine Learning Research*, 17(152):1–40.
- Tanguy, E., Flamary, R., and Delon, J. (2025). Properties of discrete sliced Wasserstein losses. *Mathematics of Computation*, 94(353):1411–1465.
- Tokdar, S. T., Zhu, Y. M., and Ghosh, J. K. (2004). Bayesian density regression with logistic Gaussian process and subspace projection. *Bayesian Analysis*, 1(1).
- Villani, C. (2009). *Optimal transport: old and new*, volume 338. Springer.

Yazar, S., Alquicira-Hernandez, J., Wing, K., Senabouth, A., Gordon, M. G., Andersen, S., Lu, Q., Rowson, A., Taylor, T. R., Clarke, L., et al. (2022). Single-cell eQTL mapping identifies cell type-specific genetic control of autoimmune disease. *Science*, 376(6589):eabf3041.

Zhao, Y., Datta, A., Tang, B., Zipunnikov, V., and Caffo, B. S. (2023). Density-on-density regression. *arXiv preprint arXiv:2307.03642*.

Supplementary Materials for “Bayesian Density-Density Regression with Application to Cell-Cell Communications”

A MCMC

We present the detail MCMC sampler for Bayesian DDR with the linear regression function:

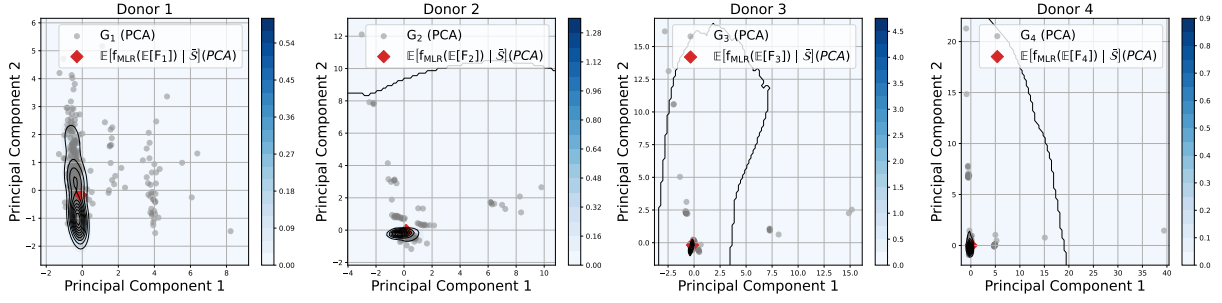
$$\lambda_{ij}^2 \mid A_{ij}, \tau \sim \text{Inverse-Gamma} \left(1, \frac{1}{\nu_{ij}} + \frac{A_{ij}^2}{2\tau^2} \right), \nu_{ij} \mid \lambda_{ij} \sim \text{Inverse-Gamma} \left(\frac{1}{2}, 1 + \frac{1}{\lambda_{ij}^2} \right), \tau^2 \mid A, \lambda_{ij}, \zeta \sim \text{Inverse-Gamma} \left(\frac{d_1+d_2}{2}, \frac{1}{\zeta} + \sum_{i=1}^{d_1} \sum_{j=1}^{d_2} \frac{A_{ij}^2}{2\lambda_{ij}^2} \right), \zeta \mid \tau \sim \text{Inverse-Gamma} \left(\frac{1}{2}, 1 + \frac{1}{\tau^2} \right),$$

and $(A, b) \sim p(A, b \mid \lambda^2, \tau^2, \mathcal{S})$.

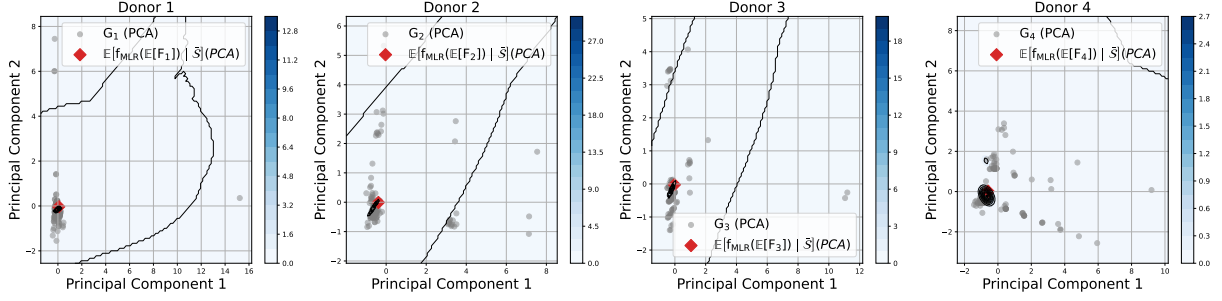
B Graph Discovery

In Figures 7-10 we show fitted means under Bayesian MLR and fitted densities under Bayesian DDR for all ordered pairs of cell types. As before, we use PCA for the response distribution of each donor to obtain a 2-dimensional projection. We observe that the predictions align with the reported RPEs shown in Figure 8 in the main text. Notably, Bayesian DDR provides more precise fits compared to Bayesian MLR, especially in cases where the response distributions are multimodal or exhibit high uncertainty.

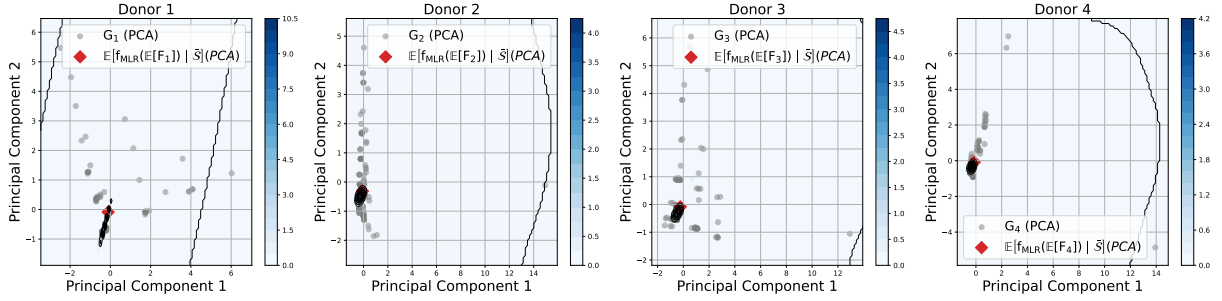
Figure 8 shows boxplots of RPE for all ordered pairs of cell types. As before, we use the intercept model as the reference f_0 for computing RPEs. Figures 11-22 show boxplots for the linear regression coefficients of all ordered pairs of cell types. Such inference allows us to identify which ligands are significant in predicting a receptor. This is done by inspecting the posterior distribution for the corresponding coefficient A_{eij} . Values far from zero indicate significant receptor/ligand pairs. Consider, for example, the regression of B cell receptor expression on T cell ligands. Both ligands, CD40L and IFN- γ are significant in predicting



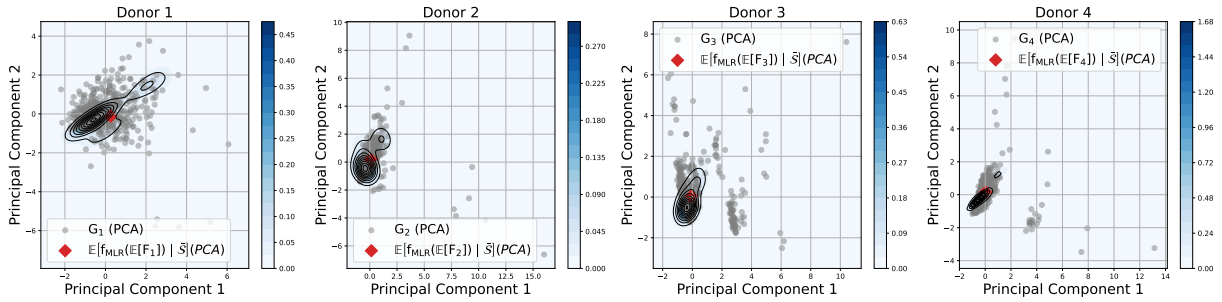
(a) B to T cells



(b) T to B cells



(c) T cells to monocytes



(d) monocytes to T cells

Figure 7: Fitted densities under Bayesian DDR and fitted means under Bayesian MLR for edges as indicated by subtitles (a) through (d). Compare with Figure 1 for an explanation of the symbols and contours.

receptors such as IGDM, IGHD, IGHG, and IL-6R. Specifically, the ligand IFN- γ appears critical to predict gene expression for the receptor IGHA, while CD40L is required to predict receptors CD40, ICOSL, IL-21R, BAFFR, CXCR5, and CCR7. Similar conclusions can

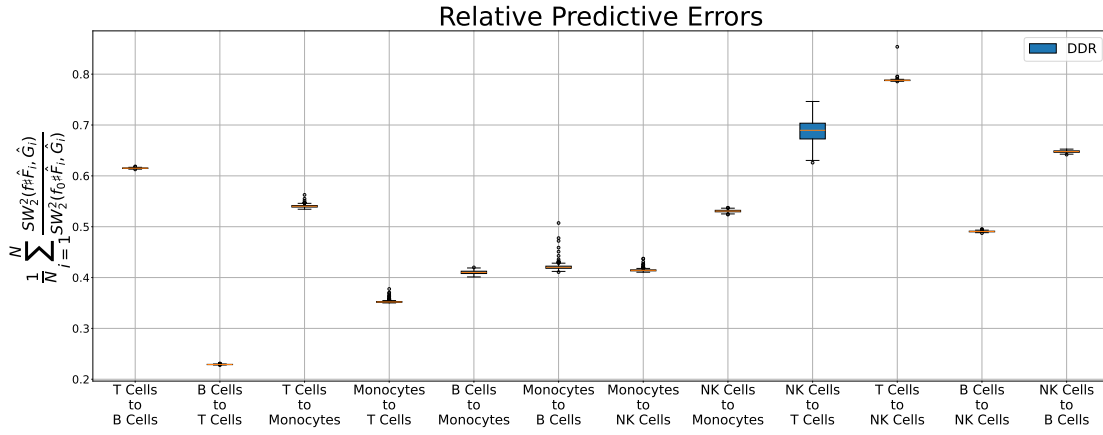
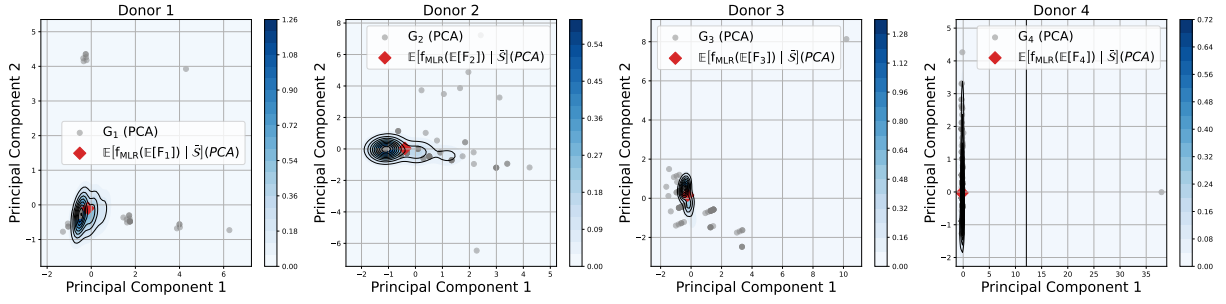


Figure 8: Boxplots of relative predictive errors for Bayesian DDR for each ordered pair of cell types on the x-axis.

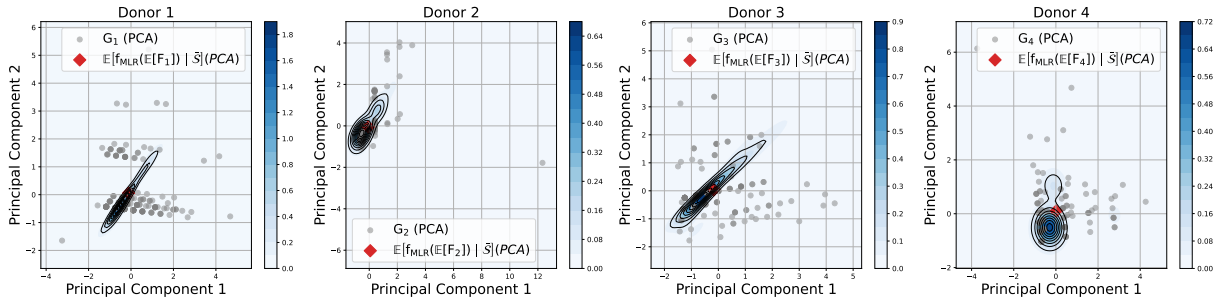
be drawn for other ligand/receptor relations. For a more formal assessment one could use pseudo inclusion probabilities like (16) to quantify the evidence for a ligand being significant in predicting a receptor.

C Semi-Simulation

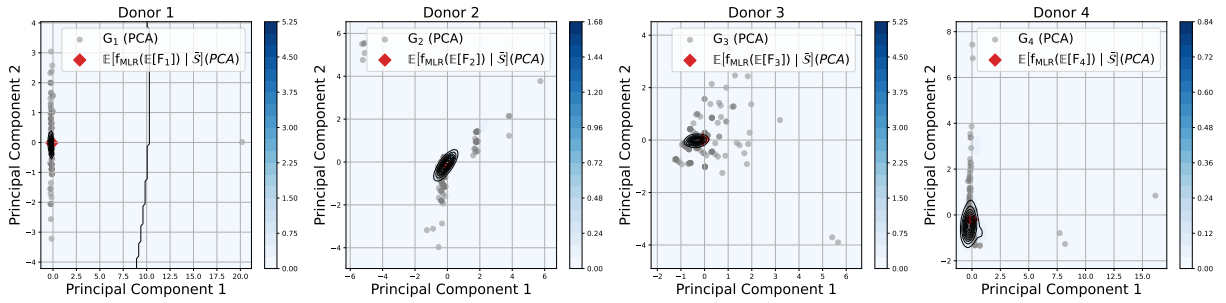
Figure 23 shows boxplots of RPEs for all pairs of cell types under the “no edge”, the “full graph”, and the “sparse graph” setting. From the low RPE values we conclude that the proposed Bayesian DDR provides acceptable fits for nearly all pairs of cell types across all three settings. Finally, Figure 24 summarizes posteriors of square errors over all coefficients of A_{eij} , b_e . Consistently small values across all three simulation scenarios indicate that Bayesian DDR provides a good fit to the semi-simulated data across all settings.



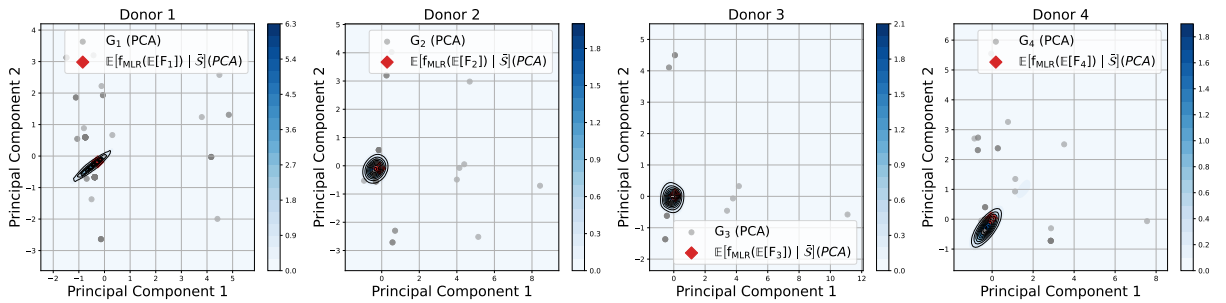
(a) B cells to monocytes



(b) monocytes to B cells

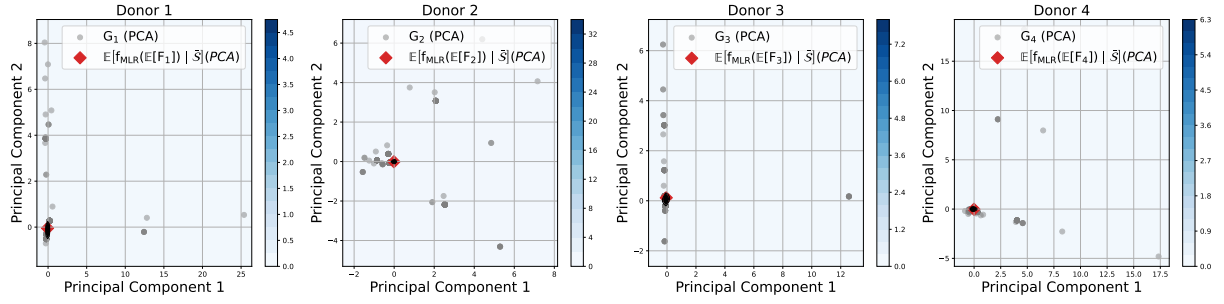


(c) monocytes to NK cells

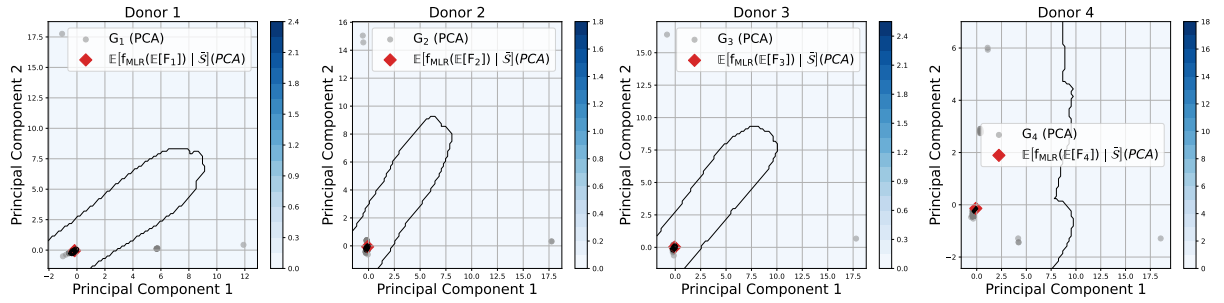


(d) NK cells to monocytes

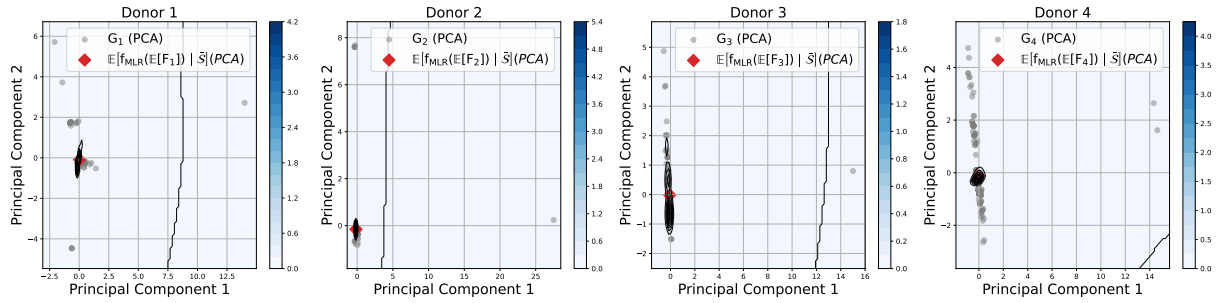
Figure 9: Same as Figure 7 for more pairs.



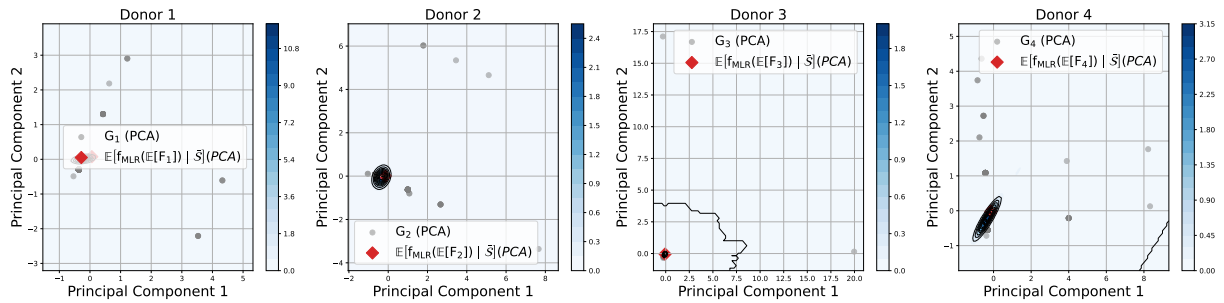
(a) NK to T cells



(b) T cells to NK cells



(c) B to NK cells



(d) NK to B cells

Figure 10: Same as Figure 7 for more pairs.

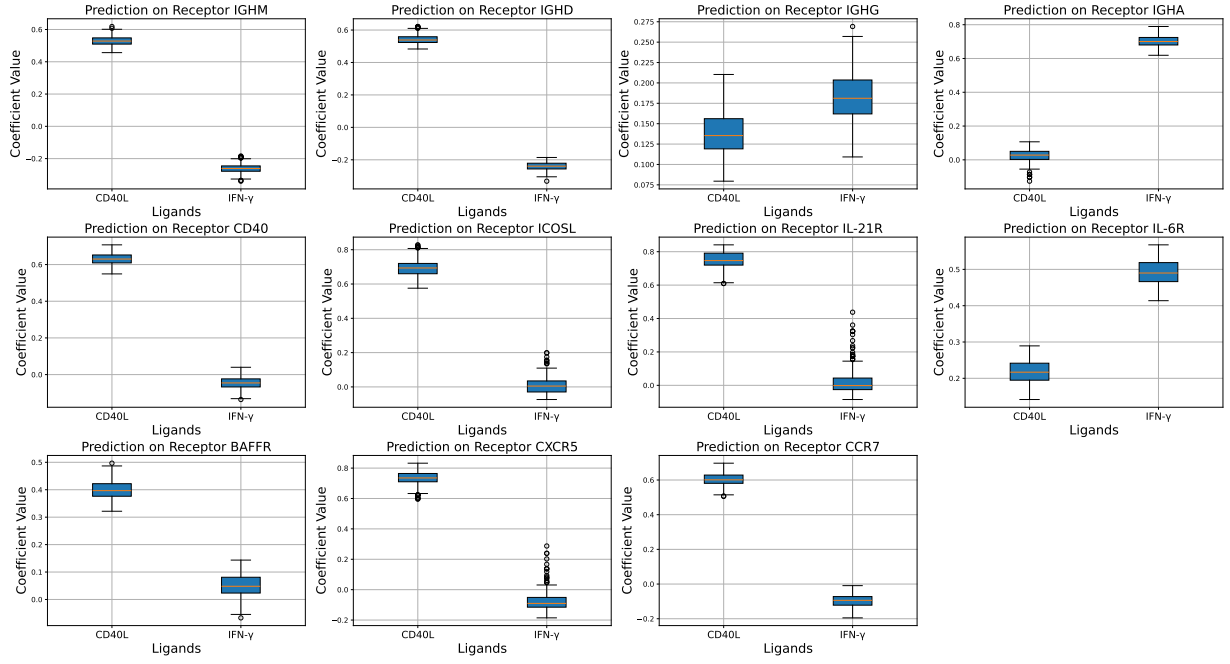


Figure 11: Boxplots of posterior samples for the coefficients of the linear regression matrix A_e for the ordered pair of cell types: T to B cells.

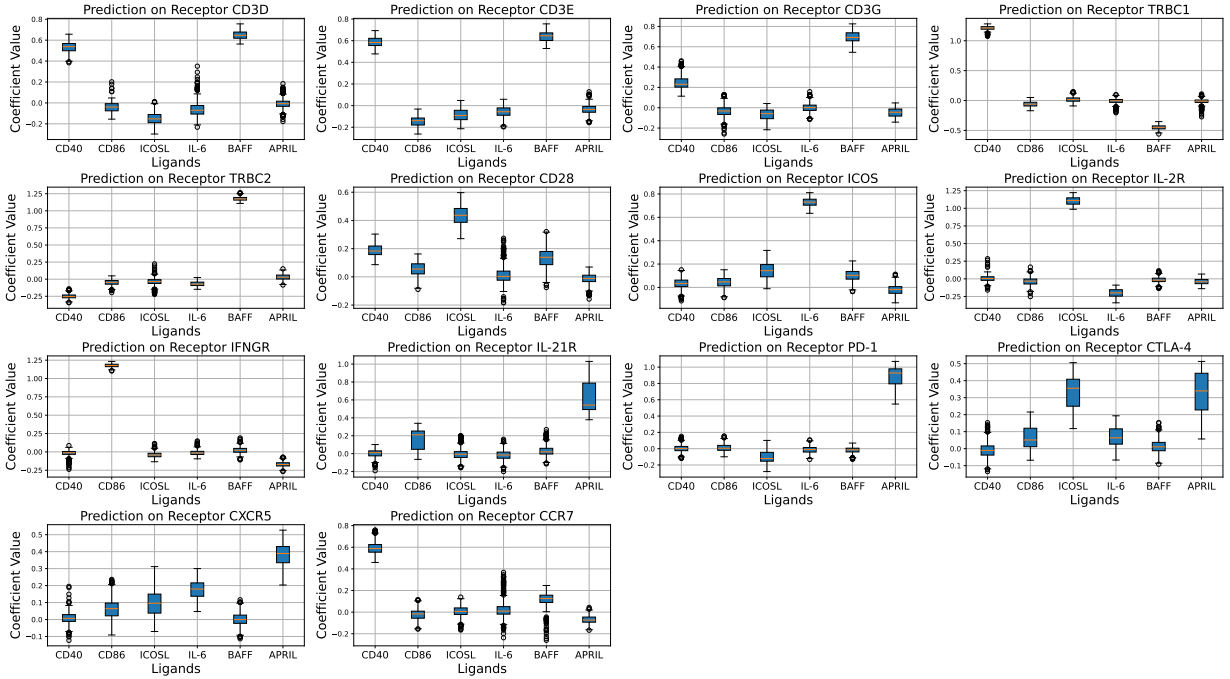


Figure 12: Same as Figure 11 for B to T cells.

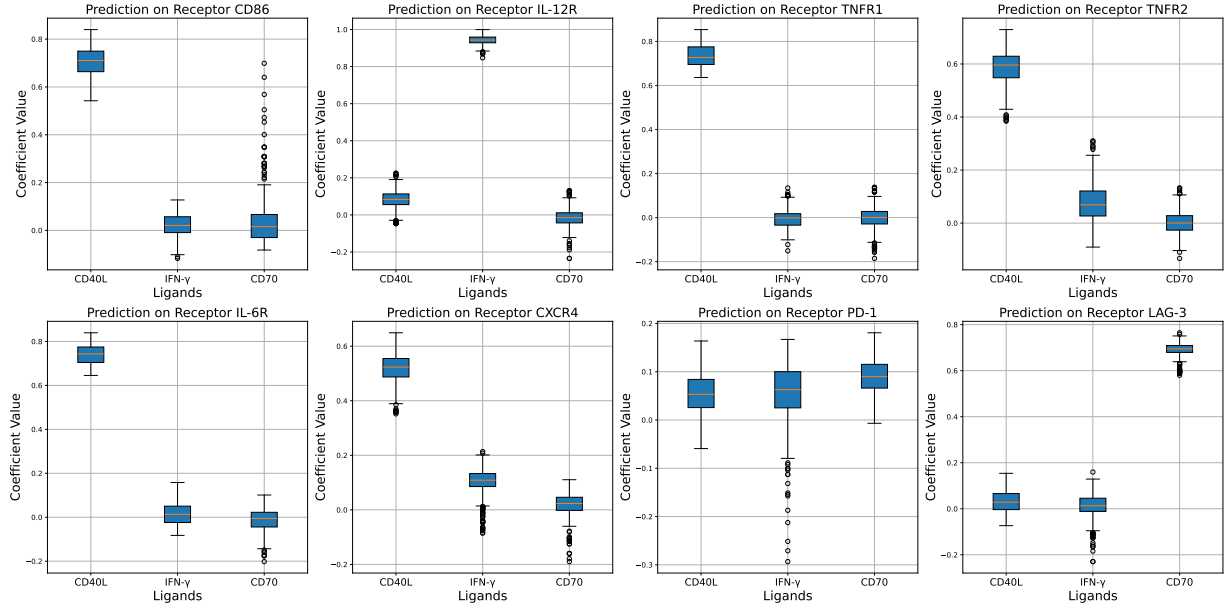


Figure 13: Same as Figure 11 for T cells to monocytes

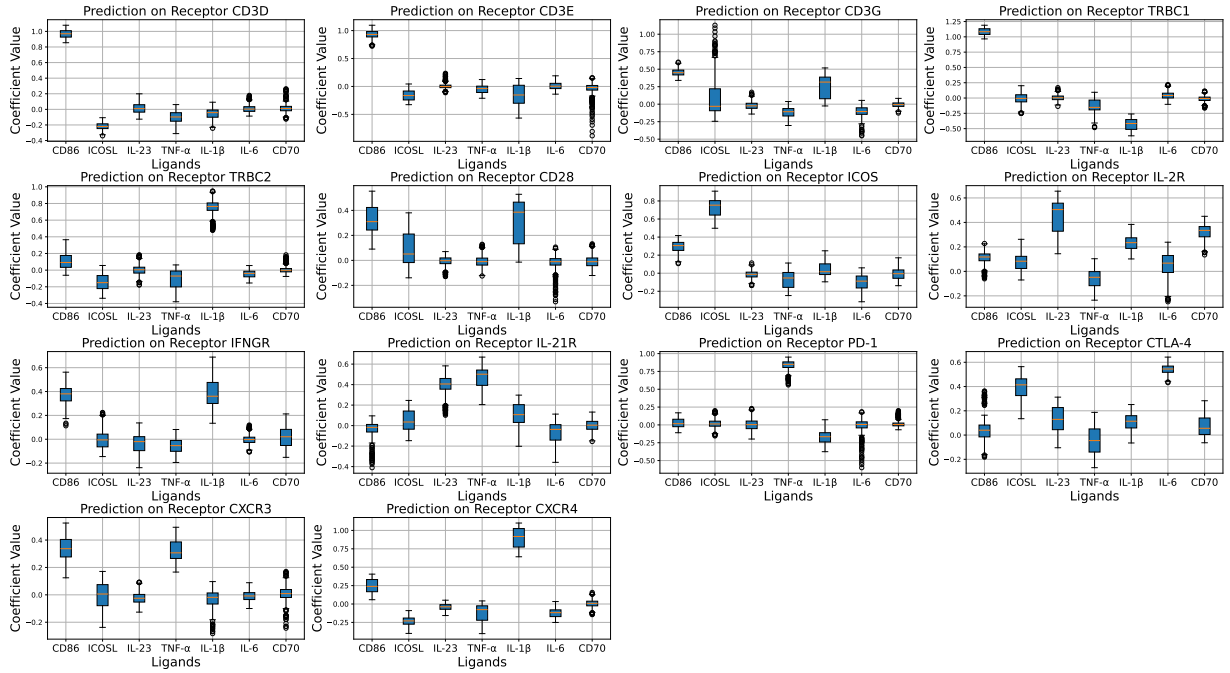


Figure 14: Same as Figure 11 for monocytes to T cells

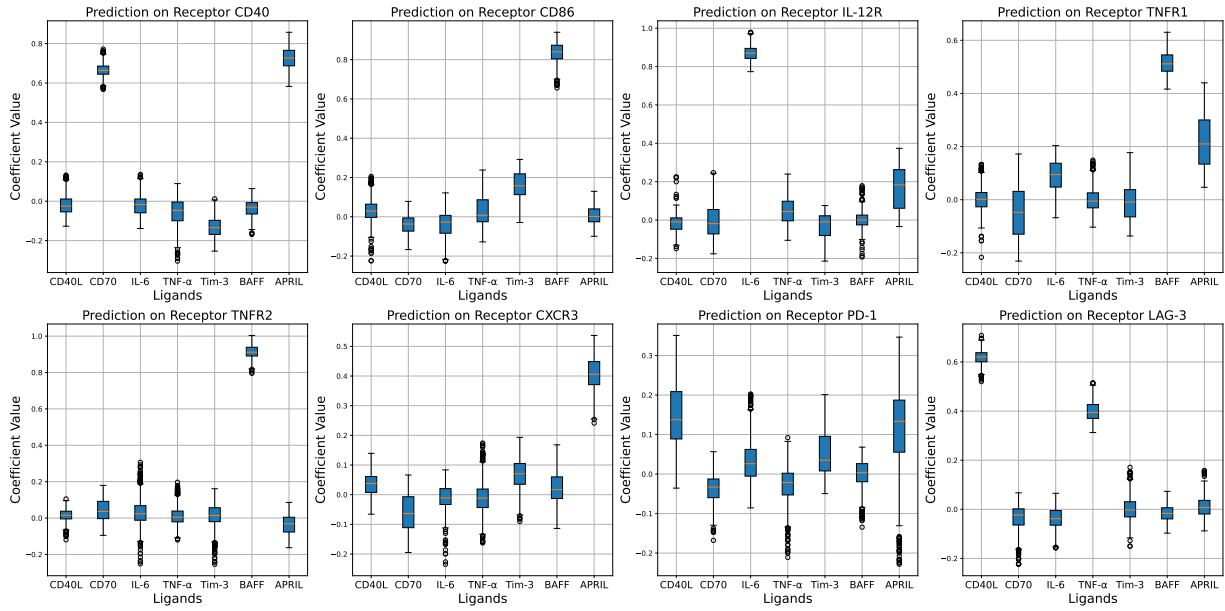


Figure 15: Same as Figure 11 for B cells to monocytes

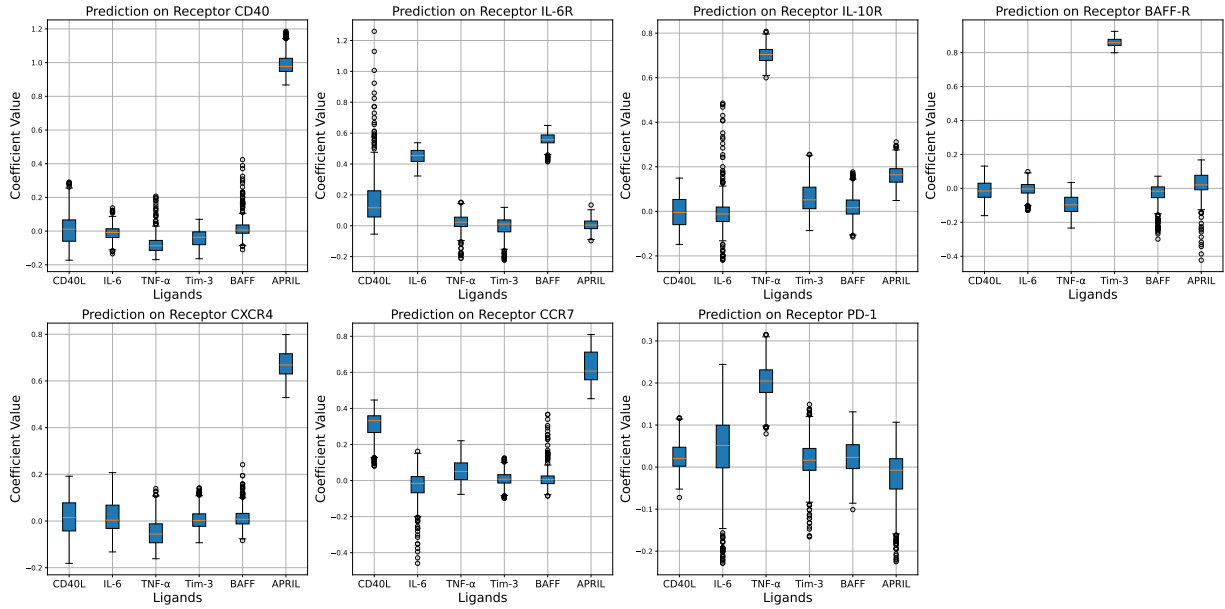


Figure 16: Same as Figure 11 for monocytes to B cells

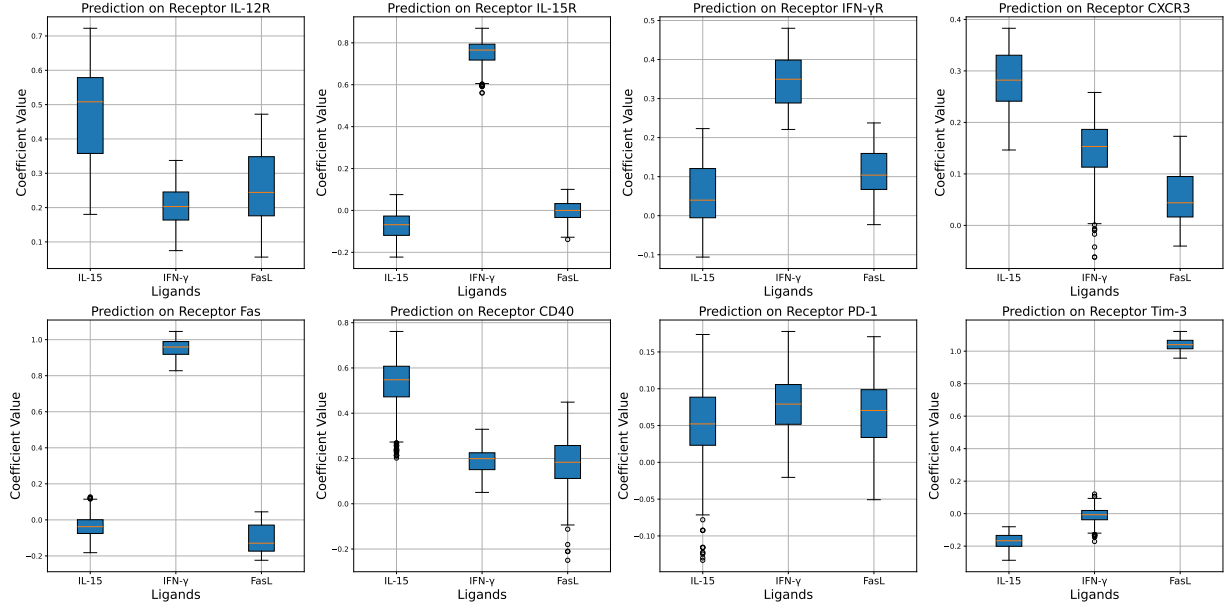


Figure 17: Same as Figure 11 for NK cells to monocytes

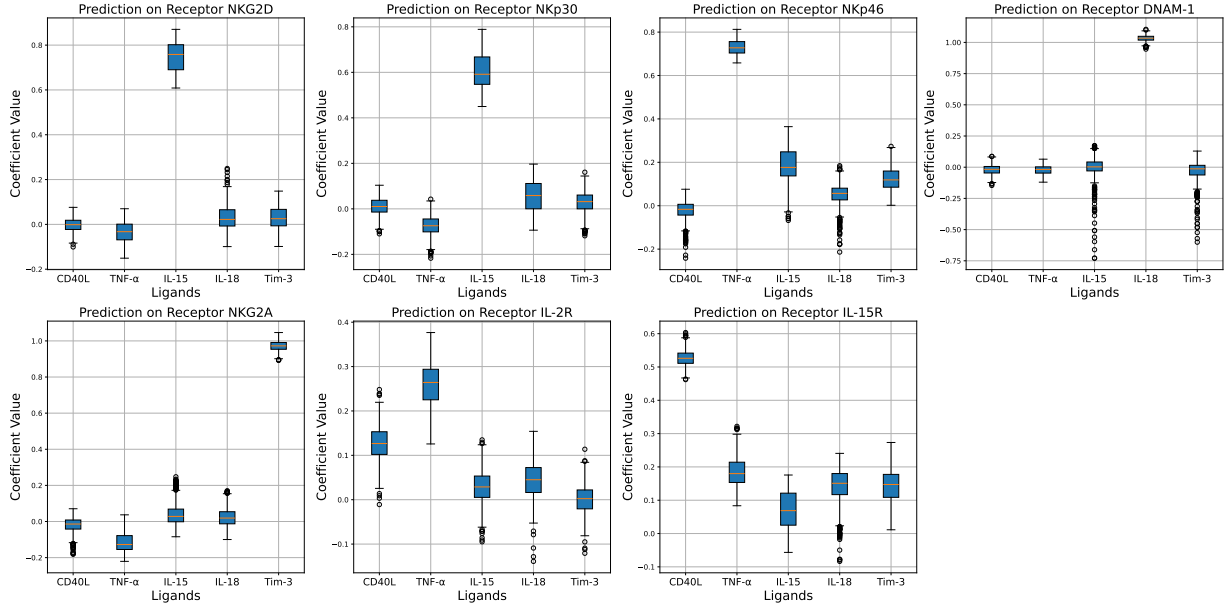


Figure 18: Same as Figure 11 for monocytes to NK cells

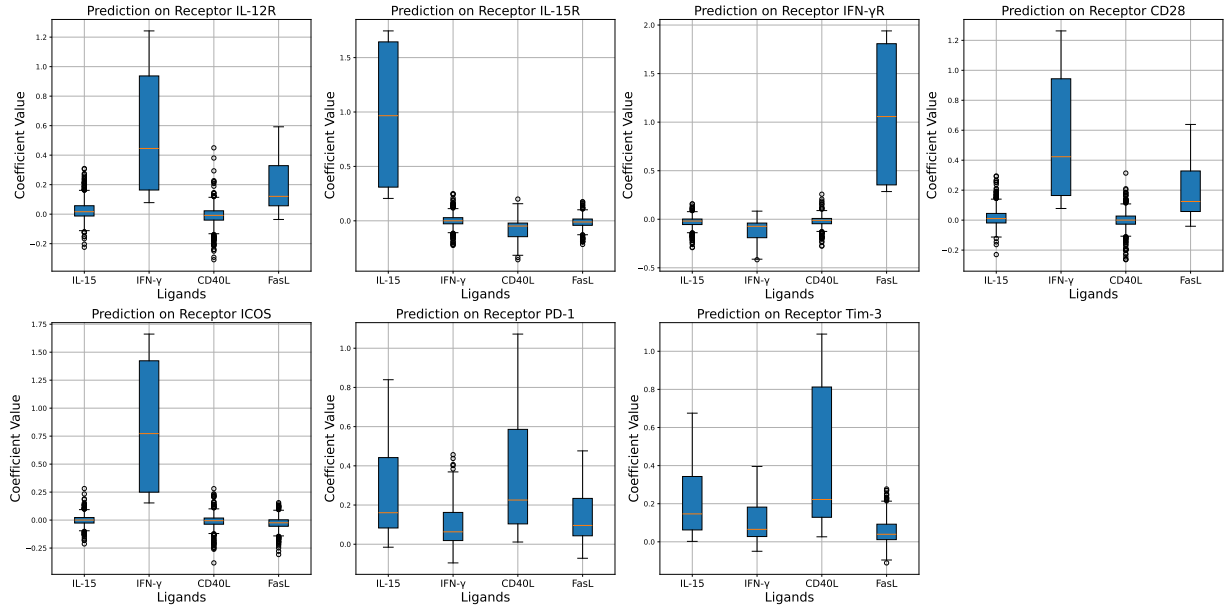


Figure 19: Same as Figure 11 for NK to T cells

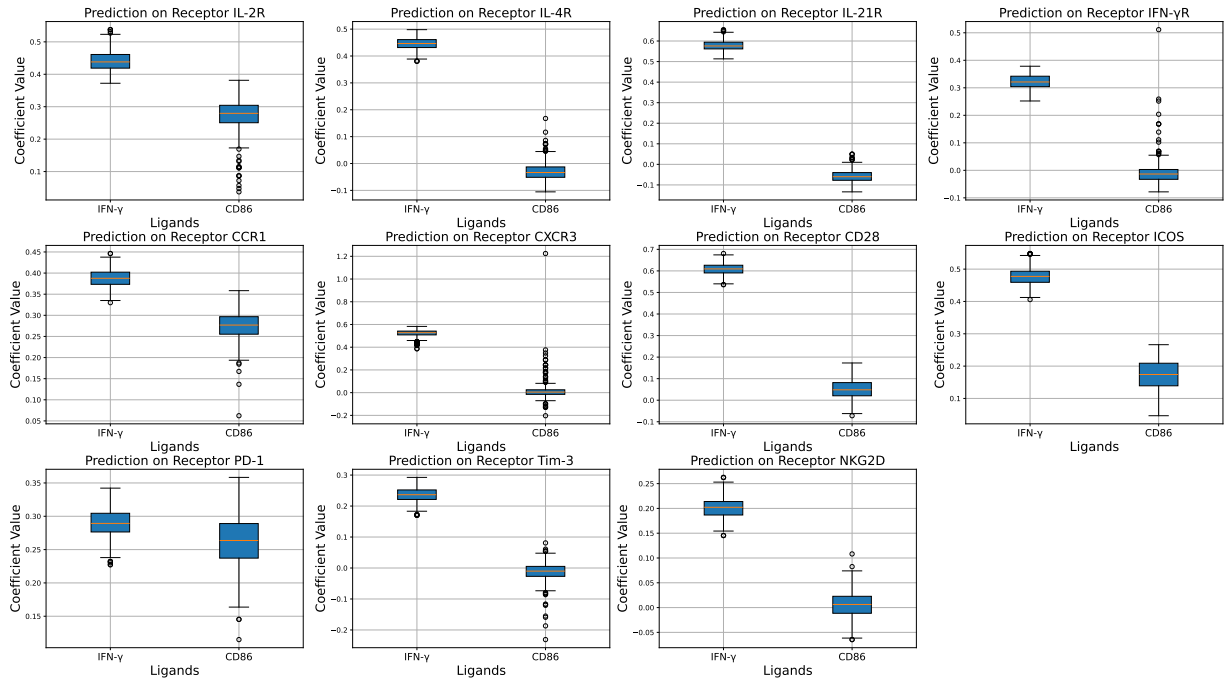


Figure 20: Same as Figure 11 for T to NK cells

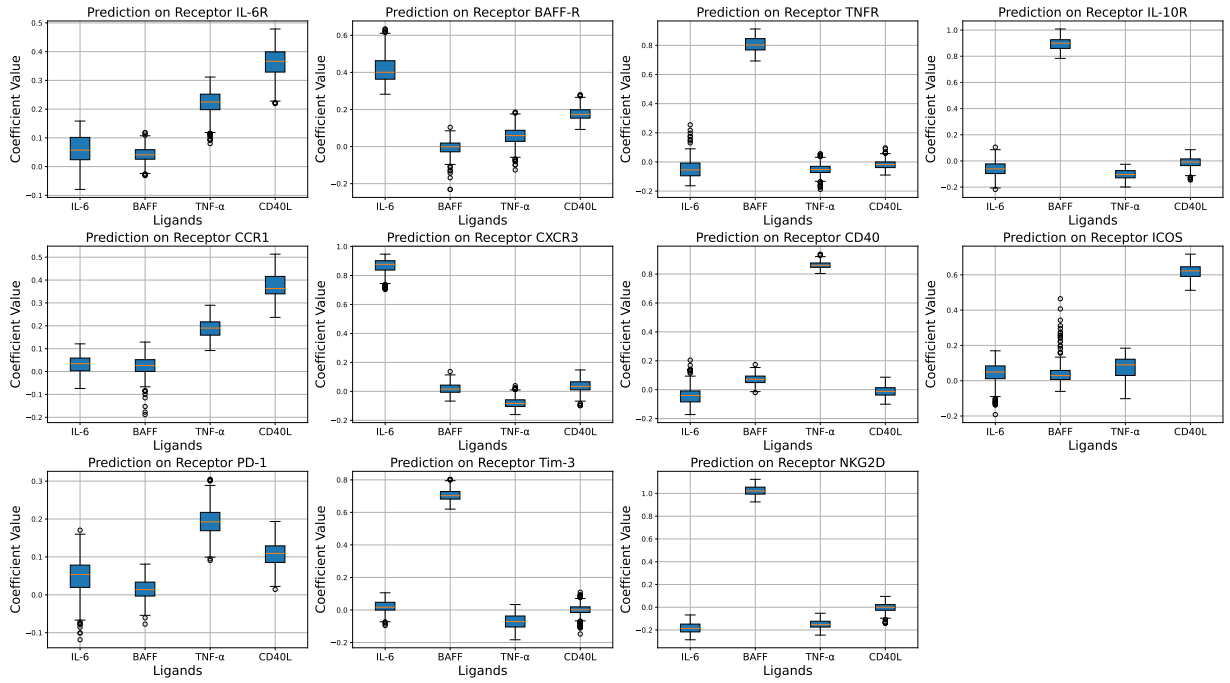


Figure 21: Same as Figure 11 for B to NK cells

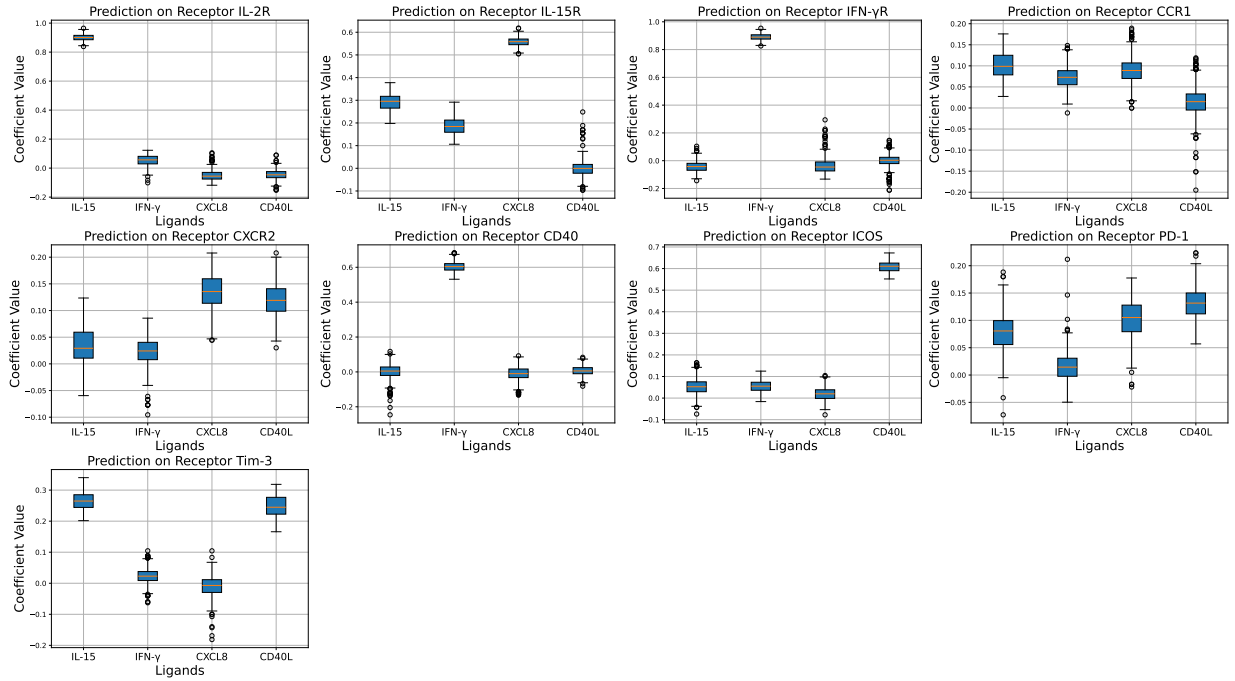


Figure 22: Same as Figure 11 for NK to B cells

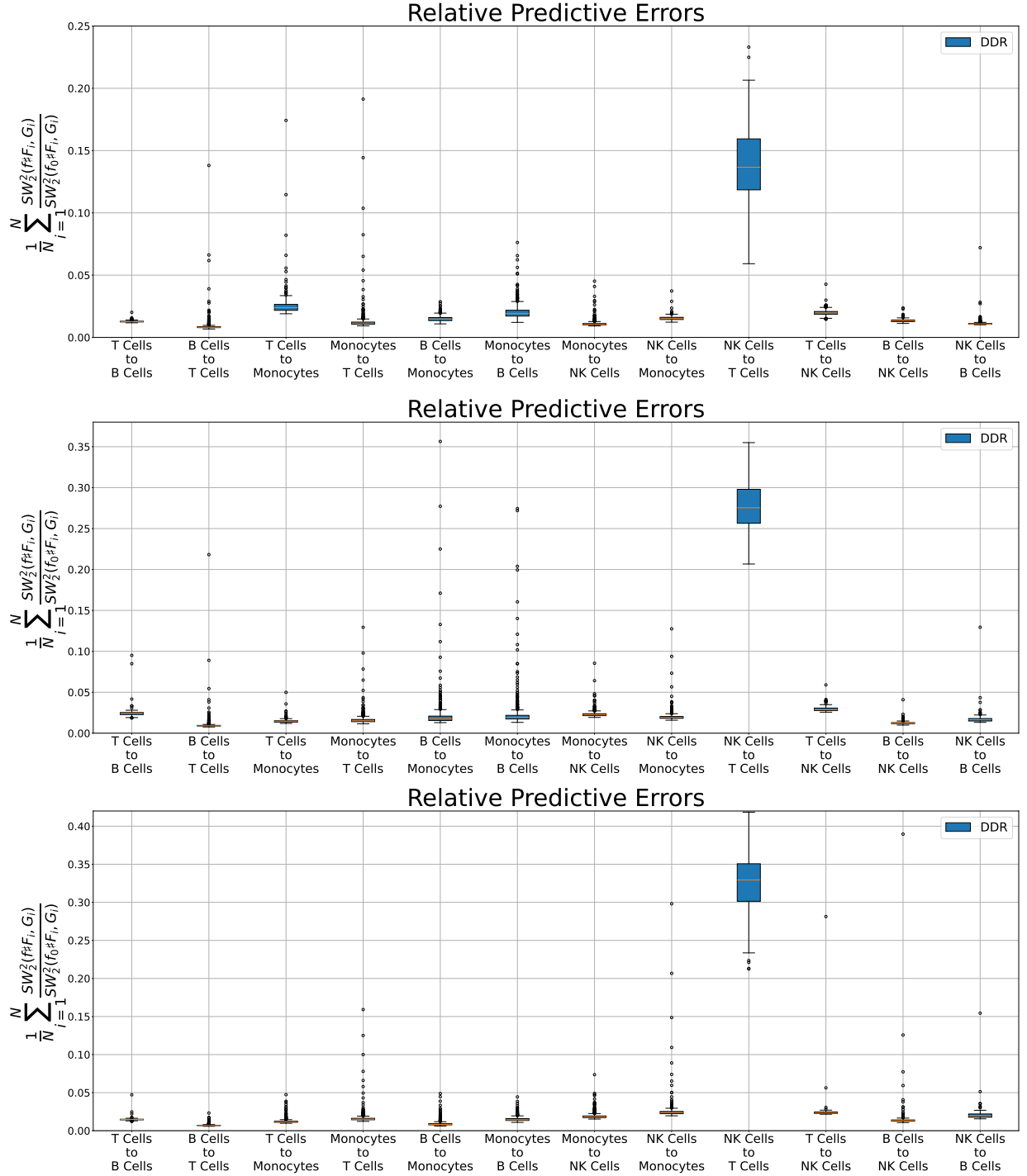


Figure 23: Boxplots of relative predictive errors (7) under the Bayesian DDR for each pair of cell types (on the horizontal axis) in the “no edge” (top), the “full graph” (middle), and the “sparse edge” simulation scenarios.

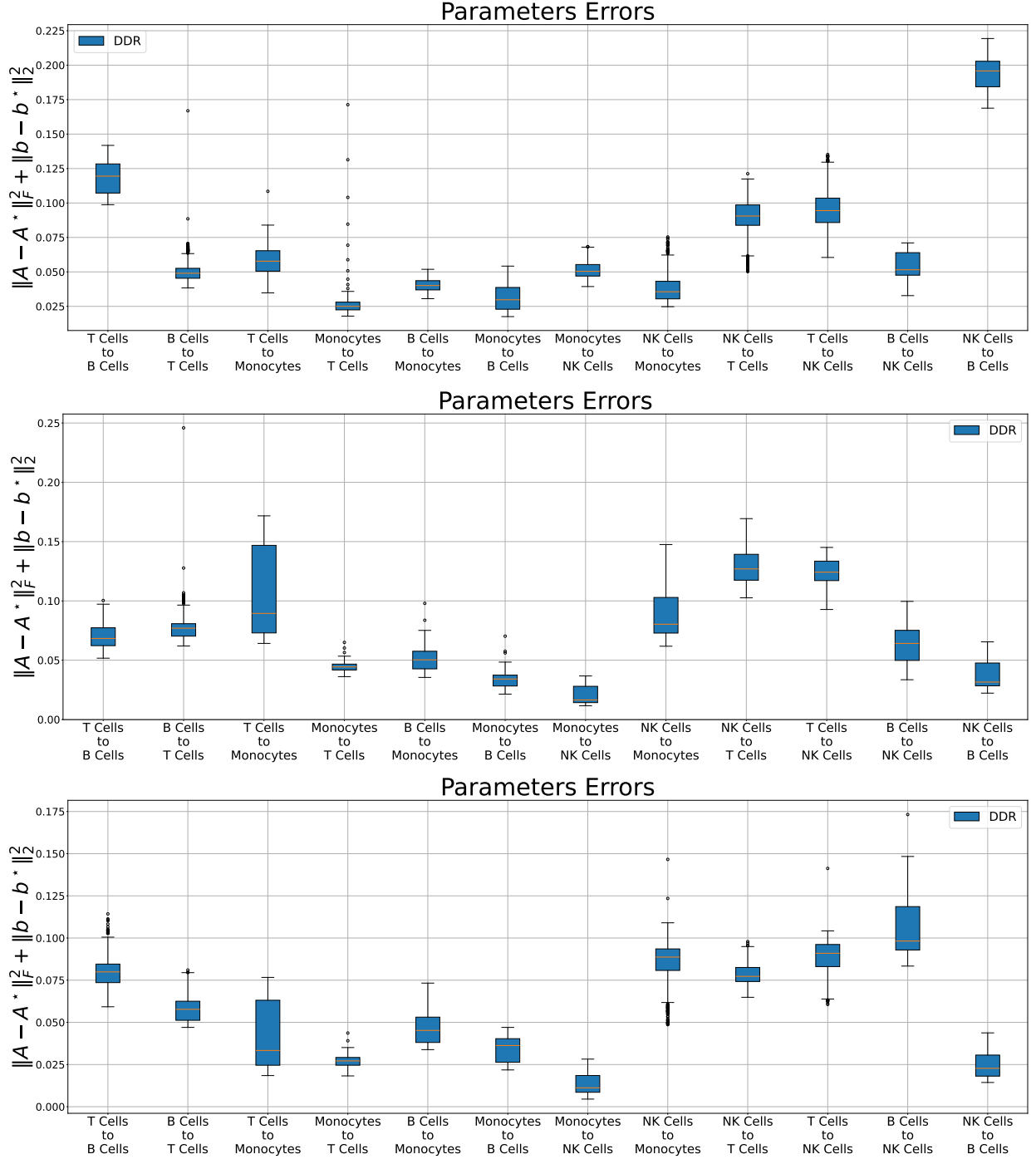


Figure 24: Boxplots of the posterior of squared errors $\|A - A^*\|_F^2 + \|b - b^*\|_2^2$, over all coefficients of A_e and b_e , arranged as in Figure 23.